Three-dimensional Landau theory for multivariant stress-induced martensitic phase transformations. III. Alternative potentials, critical nuclei, kink solutions, and dislocation theory

Valery I. Levitas,[1,*] Dean L. Preston,[2] and Dong-Wook Lee[1]
[1]*Texas Tech University, Center for Mechanochemistry and Synthesis of New Materials, Department of Mechanical Engineering, Lubbock, Texas 79409-1021, USA*
[2]*Applied Physics Division, Los Alamos National Laboratory, Los Alamos, New Mexico 87545, USA*
(Received 2 April 2003; published 6 October 2003)

In part III of this paper, alternative Landau potentials for the description of stress-and temperature-induced martensitic phase transformations under arbitrary three-dimensional loading are obtained. These alternative potentials include a sixth-degree (2-4-6) polynomial in Cartesian order parameters and a potential in hyperspherical order parameters. Each satisfies all conditions for the correct description of experiments. The unique features of the potentials are pointed out and a detailed comparison of the potentials is made for NiAl alloy. Analytic solutions of the one-dimensional time-independent Ginzburg-Landau equations for the 2-3-4 and 2-4-6 potentials for a constant-stress tensor and invariant-plane strain are obtained and compared. Solutions include martensitic and austenitic critical nuclei and diffuse martensite-austenite and martensite-martensite interfaces. The widths and energies of the nuclei and interfaces are functions of the thermodynamic driving force, the gradient energy coefficient, and a parameter that characterizes the stability of austenite. The splitting of a martensite-martensite interface into two austenite-martensite interfaces is interpreted as a potentially new mechanism—namely, barrierless austenite nucleation—which might be observed experimentally at the interface between two invariant-plane-strain variants. The widths, energies, and gradient energy coefficients of the martensite-martensite and austenite-martensite interfaces are estimated for NiAl. Finally, we outline a version of phase field theory for dislocations based on our theoretical framework for phase transformations.

DOI: 10.1103/PhysRevB.68.134201 PACS number(s): 64.60.−i

I. INTRODUCTION

In parts I (Ref. 1) and II (Ref. 2) we developed a fifth-degree polynomial (2-3-4-5) Gibbs (Landau) potential for the description of multivariant stress- and temperature-induced martensitic phase transformations (PT's) in three dimensions. Our approach was a phenomenological one; that is, the 2-3-4-5 potential was constructed by requiring that it respects the experimentally observed features of martensitic PT's in shape memory alloys and steels, specifically, constant transformation strain, weakly temperature dependent, or constant, stress hysteresis, and transformation at nonzero tangent elastic moduli. However, the 2-3-4-5 potential is by no means the only Landau potential that satisfies these basic requirements. In this paper, we develop three alternative potentials: namely, a 2-4-6 polynomial in Cartesian order parameters (Sec. II) and two potentials in hyperspherical order parameters (Sec. III). The symmetry requirements for the Gibbs potential (see Sec. IV in Ref. 2) are satisfied for the potentials derived in this paper. The phase equilibrium and transformation conditions for all potentials, including the 2-3-4-5 potential, are identical. Consequently, the geometric representations of the phase equilibrium and transformation conditions introduced in part II Ref. 2 can be used for the alternative potentials as well.

The distinguishing feature of the 2-4-6 polynomial is that its curvature at the martensitic (M) minimum is 4 times larger than at the austenitic (A) minimum, while both curvatures are the same for the 2-3-4-5 polynomial derived in Refs. 1 and 2. This difference in the curvatures significantly modifies the profiles of 2-4-6 critical martensitic nuclei relative to the corresponding profiles for the 2-3-4-5 potential. In contrast to the 2-3-4-5 and 2-4-6 potentials, the hyperspherical potentials have no unphysical local minima and have no constants that do not appear in the phase equilibrium and transformation conditions. Variant-variant transformations occur along the unit hypersphere, whereas the variant-variant transformation paths are much more complicated for the 2-3-4-5 and 2-4-6 polynomial potentials.

It is shown for all potentials that the number of order parameters can be reduced by a factor of 2 if transformation strains for pairs of martensitic variants decompose into two components: one that is the same for both variants and one that is equal in magnitude but of opposite sign for the two variants. This allows us to reduce the number of order parameters by a factor of 2. Examples of applications include cubic-orthorhombic, cubic-monoclinic-I, and cubic-monoclinic-II PT's and PT's of invariant-plane-strain (IPS) variants.

In Sec. IV, we compare the 2-3-4-5, 2-4-6, and polar 2-3-4 potentials for the NiAl cubic-tetragonal phase transformation for zero stress and for two three-dimensional stress states.

In Sec. V, analytical solutions of the one-dimensional static Ginzburg-Landau equations for a constant three-dimensional stress tensor and invariant-plane strain are found for the 2-3-4 and 2-4-6 potentials and compared. Analytical solutions of the Ginzburg-Landau equation for the 2-4-6 potential in strain for the stress-free case were found by Falk.[5] Jacobs[6] generalized some of them to finite strain and to two-dimensional problems that can be treated as one dimensional

and also calculated displacements. However, the physical interpretation of some of the solutions, such as solitons on A and M and soliton splitting, was unclear. In Ref. 7, numerical solutions for critical M nuclei of the 2-3-4 potential were analyzed in detail under prescribed displacements. It was used in Ref. 7 to model the nonclassical nucleation of an ellipsoidal region.

In contrast to Refs. 5 and 6, our theory incorporates homogeneous multiaxial stresses and we provide physical interpretations of the solutions of the Ginzburg-Landau equations. Despite the significant differences between our theory and Falk's,[5] the dimensionless forms of the Ginzburg-Landau equations for our 2-4-6 potential and Falk's strain-based potential coincide. This enables us to borrow some of Falk's analytical solutions for the stress-free case and analyze their counterparts in relevant variables and under a constant-stress tensor, which is significantly different from Falk's results. Analytical solutions for the 2-3-4 potential are found. All solutions depend on three parameters: s_1, which characterizes the stability of austenite; s_2, which is proportional to the thermodynamic driving force for the M→A PT (both s_1 and s_2 are stress and temperature dependent); and the gradient energy coefficient β. Phase and transformation diagrams in s_1-s_2 coordinates are analyzed. It is proven by numerical solution of the time-dependent Ginzburg-Landau equation that a stationary M soliton on A and an A soliton on M are in fact martensitic and austenitic critical nuclei. The structure and energetics of the M and A critical nuclei, as well as diffuse A-M and M_+-M_- interfaces, are studied in detail. In particular, the widths of the M and A critical nuclei, and the thicknesses of their interfaces, and the energies of the nuclei, and their interfaces are determined in terms of the aforementioned three parameters. A relation between the energy and the width of the equilibrium A-M interface and stress hysteresis is found. Two types of M_+-M_- interfaces are considered: a simple kink connecting M_+ to M_- and an exotic split M_+-M_- interface comprised of juxtaposed M_+-A and A-M_- interfaces. This splitting is interpreted as a potentially new mechanism: barrierless A nucleation. Nucleation occurs in the region of stability of M near the equilibrium M-A line. Such nucleation might be found experimentally at the interface between two IPS variants.

In Sec. VI, the gradient energy coefficients, energies, and widths of the M_+-M_- and A-M interfaces are estimated for NiAl alloy.

In Sec. VII, a phase field theory of dislocations is developed. The known theory[3] is based on a formalism similar to phase field theory of martensitic PT's (Ref. 4) and has a similar shortcoming; namely, the equilibrium value of the Burgers vector and the plastic strain depend on stress. We extend our approach developed for PT's to dislocations to eliminate this drawback.

II. SIXTH-DEGREE POLYNOMIAL GIBBS POTENTIAL

In this section we obtain a sixth-degree polynomial Gibbs potential G that describe PT's between austenite (A) and martensitic variants (M_i, $i=1,2,\ldots,n$) and between martensitic variants. One of the requirements of G is that it describe PT's with transformation strains that differ only in sign. This is usually done by means of an even polynomial potential in the strain.[8,6] The only strain appearing in our Landau potentials is the transformation strain $\boldsymbol{\varepsilon}_t$, but it cannot serve as an order parameter because it does not change with the stress, like the strain does—the transformation strain is fixed for each martensitic variant. To describe a change in sign of the transformation strain, the function φ [see Eqs. (1) and (2)] must be odd in the order parameter η, but the thermal part of the free energy f must be an even function of η. If $\varphi(\eta)$ is a 1-3-5 polynomial and $f(\eta)$ is a 2-4-6 polynomial, then $G(\eta)$ is a complete (contains all powers) sixth-degree polynomial that cannot be studied analytically and may have additional unwanted extrema. There is, however, an alternative to including odd powers of η: $\boldsymbol{\varepsilon}_t \mathrm{sgn}(\eta)$ is substituted for $\boldsymbol{\varepsilon}_t$ in a 2-4-6 polynomial Gibbs potential.

In Sec. II A we derive a 2-4-6 polynomial potential in order parameters $\eta_i \in [0,1]$. In Sec. II B the range of order parameter values is extended from $[0,1]$ to $[-1,1]$ for PT's with $\boldsymbol{\varepsilon}_t$ that differ only in sign and more generally for PT's where the $\boldsymbol{\varepsilon}_t$ for pairs of martensitic variants decompose into two components: one that is the same for both variants and one that is equal in magnitude but of opposite sign for the two variants. This extension reduces the number of order parameters by a factor of 2. A similar result was obtained for the 2-3-4-5 potential.

A. Positive order parameters

The 2-4-6 polynomial is subject to the same requirements as the 2-3-4-5 polynomial Gibbs potential derived in parts I (Refs. 1) and II (Ref. 2). Following the same steps as before we obtain

$$\begin{aligned} G = &- \boldsymbol{\sigma}\!:\!\left(\boldsymbol{\lambda}_0 + \sum_{k=1}^{n} (\boldsymbol{\lambda}_k - \boldsymbol{\lambda}_0)\ \ \varphi(a_\lambda, \eta_k) \right)\!:\!\boldsymbol{\sigma}/2 \\ &- \boldsymbol{\sigma}\!:\!\left(\left(\boldsymbol{\lambda}_0^3 + \sum_{k=1}^{n} (\boldsymbol{\lambda}_k^3 - \boldsymbol{\lambda}_0^3)\varphi(a_{3\lambda}, \eta_k) \right)\!:\!\boldsymbol{\sigma} \right)\!:\!\boldsymbol{\sigma}/3 \\ &- \boldsymbol{\sigma}\!:\!\left(\boldsymbol{\sigma}\!:\!\left(\boldsymbol{\lambda}_0^4 + \sum_{k=1}^{n} (\boldsymbol{\lambda}_k^4 - \boldsymbol{\lambda}_0^4)\varphi(a_{4\lambda}, \eta_k) \right)\!:\!\boldsymbol{\sigma} \right)\!:\!\boldsymbol{\sigma}/4 \\ &- \boldsymbol{\sigma}\!:\!\sum_{k=1}^{n} \boldsymbol{\varepsilon}_{tk}\varphi(a, \eta_k) - \boldsymbol{\sigma}\!:\!\left(\boldsymbol{\varepsilon}_{\theta 0} + \sum_{k=1}^{n} (\boldsymbol{\varepsilon}_{\theta k} - \boldsymbol{\varepsilon}_{\theta 0})\varphi(a_\theta, \eta_k) \right) \\ &+ \sum_{k=1}^{n} f(\theta, \eta_k) + \sum_{i=1}^{n-1} \sum_{j=i+1}^{n} F_{ij}(\eta_i, \eta_j); \end{aligned} \tag{1}$$

$$\varphi(a, \eta_k) = a\,\eta_k^2/2 + (3-a)\,\eta_k^4 + (a-4)\,\eta_k^6/2, \quad 0 \leqslant a \leqslant 6; \tag{2}$$

$$f(\theta, \eta_k) = A\,\eta_k^2/2 + (3\Delta G^\theta - A)\,\eta_k^4 + (A - 4\Delta G^\theta)\,\eta_k^6/2; \tag{3}$$

$$\begin{aligned} F_{ij}(\eta_i, \eta_j) = &B\,\eta_i^2\,\eta_j^2 + (Z_{ij} - B)\,\eta_i^4\,\eta_j^2 + C\,\eta_i^3\,\eta_j^3 \\ &+ (Z_{ji} - B)\,\eta_i^2\,\eta_j^4; \end{aligned} \tag{4}$$

$$
\begin{aligned}
Z_{ij}=&\frac{a}{2}\boldsymbol{\sigma}:\boldsymbol{\varepsilon}_{tj}-\frac{3}{2}\boldsymbol{\sigma}:(\boldsymbol{\varepsilon}_{tj}-\boldsymbol{\varepsilon}_{ti})\\
&+\boldsymbol{\sigma}:\left[\frac{a_\theta}{2}(\boldsymbol{\varepsilon}_{\theta j}-\boldsymbol{\varepsilon}_{\theta 0})-\frac{3}{2}(\boldsymbol{\varepsilon}_{\theta j}-\boldsymbol{\varepsilon}_{\theta i})\right]\\
&+\boldsymbol{\sigma}:\left[\frac{a_\lambda}{4}(\boldsymbol{\lambda}_j-\boldsymbol{\lambda}_0)-\frac{3}{4}(\boldsymbol{\lambda}_j-\boldsymbol{\lambda}_i)\right]:\boldsymbol{\sigma}\\
&+\left(\boldsymbol{\sigma}:\left[\frac{a_{3\lambda}}{6}(\boldsymbol{\lambda}_j^3-\boldsymbol{\lambda}_0^3)-\frac{1}{2}(\boldsymbol{\lambda}_j^3-\boldsymbol{\lambda}_i^3)\right]:\boldsymbol{\sigma}\right):\boldsymbol{\sigma}\\
&+\boldsymbol{\sigma}:\left(\boldsymbol{\sigma}:\left[\frac{a_{4\lambda}}{8}(\boldsymbol{\lambda}_j^4-\boldsymbol{\lambda}_0^4)-\frac{3}{8}(\boldsymbol{\lambda}_j^4-\boldsymbol{\lambda}_i^4)\right]:\boldsymbol{\sigma}\right):\boldsymbol{\sigma}\\
&+\overline{A}/2-A/2. \qquad (5)
\end{aligned}
$$

Here $\boldsymbol{\sigma}$ is the stress tensor, $\boldsymbol{\varepsilon}_{ti}$ and $\boldsymbol{\varepsilon}_{\theta i}$ are the transformation and thermal strains of the ith variant, $i=0$ corresponds to A, $\boldsymbol{\varepsilon}_{t0}=\mathbf{0}$, $\boldsymbol{\lambda}_i^k$ is the elastic compliance tensor of order k for variant i ($\boldsymbol{\lambda}_i\equiv\boldsymbol{\lambda}_i^2$), and ΔG^θ is the difference between the thermal parts of the Gibbs energies of M and A. The parameters A and $\overline{A}$ characterize the thresholds for $\mathsf{A}\leftrightarrow\mathsf{M}_i$ and $\mathsf{M}_j\leftrightarrow\mathsf{M}_i$ transformations, while B and C control the Gibbs energy away from both the A and M_i minima and the minimum-energy paths between the minima; therefore, they do not affect phase equilibrium and transformation conditions. The material parameters a, a_θ, $a_{2\theta}$, $a_{3\theta}$, and $a_{4\theta}$ govern the variations of $\boldsymbol{\varepsilon}_{ti}$, $\boldsymbol{\varepsilon}_{\theta i}$, and the elastic compliances between the A and M_i minima.

Define $\hat{\eta}_i=(0,\ldots,0,\eta_i=1,0,\ldots,0)$, the vector from the origin to M_i. The Gibbs potential was constructed to have local minima at the origin and at the points $\hat{\eta}_i$, $i=1,\ldots,n$, but no constraints were placed on G at the points $\hat{\eta}_i+\hat{\eta}_j$, $\hat{\eta}_i+\hat{\eta}_j+\hat{\eta}_k$, etc. Consequently, G may be smaller at such points that at the A and M_i local minima; i.e., nonphysical phases can appear. The relative values of G at A, M_i, $\hat{\eta}_i+\hat{\eta}_j$, etc., are controlled by the parameters B and C. Since $F_{ij}(1,1)=Z_{ij}+Z_{ji}-B+C$, the elimination of minima at $\hat{\eta}_i+\hat{\eta}_j$, $\hat{\eta}_i+\hat{\eta}_j+\hat{\eta}_k$, etc., can be achieved by choosing $B\leqslant 0$ and $C>0$.

Define $\overline{0}=(0,\ldots,0)$, which corresponds to A, and $\overline{\eta_i}=(0,\ldots,0,\eta_i,0,\ldots,0)$. The phase transformation conditions are as follows:

$\mathsf{A}\rightarrow\mathsf{M}_i$:

$$
\begin{aligned}
&\frac{\partial^2 G(\boldsymbol{\sigma},\theta,\overline{0})}{\partial\eta_i^2}\leqslant 0\\
&\quad\Rightarrow a\,\boldsymbol{\sigma}:\boldsymbol{\varepsilon}_{ti}+a_\theta\boldsymbol{\sigma}:(\boldsymbol{\varepsilon}_{\theta i}-\boldsymbol{\varepsilon}_{\theta 0})+\frac{a_\lambda}{2}\boldsymbol{\sigma}:(\boldsymbol{\lambda}_i-\boldsymbol{\lambda}_0):\boldsymbol{\sigma}\\
&\qquad+\frac{a_{3\lambda}}{3}\boldsymbol{\sigma}:((\boldsymbol{\lambda}_i^3-\boldsymbol{\lambda}_0^3):\boldsymbol{\sigma}):\boldsymbol{\sigma}\\
&\qquad+\frac{a_{4\lambda}}{4}\boldsymbol{\sigma}:(\boldsymbol{\sigma}:(\boldsymbol{\lambda}_i^4-\boldsymbol{\lambda}_0^4):\boldsymbol{\sigma}):\boldsymbol{\sigma}\geqslant A;
\end{aligned}
$$

$\mathsf{M}_i\rightarrow\mathsf{A}$:

$$
\begin{aligned}
&\frac{\partial^2 G(\boldsymbol{\sigma},\theta,\widehat{\eta_i})}{\partial\eta_i^2}\leqslant 0\\
&\quad\Rightarrow(6-a)\,\boldsymbol{\sigma}:\boldsymbol{\varepsilon}_{ti}+(6-a_\theta)\,\boldsymbol{\sigma}:(\boldsymbol{\varepsilon}_{\theta i}-\boldsymbol{\varepsilon}_{\theta 0})\\
&\qquad+\frac{6-a_\lambda}{2}\boldsymbol{\sigma}:(\boldsymbol{\lambda}_i-\boldsymbol{\lambda}_0):\boldsymbol{\sigma}\\
&\qquad+\frac{6-a_{3\lambda}}{3}\boldsymbol{\sigma}:((\boldsymbol{\lambda}_i^3-\boldsymbol{\lambda}_0^3):\boldsymbol{\sigma}):\boldsymbol{\sigma}\\
&\qquad+\frac{6-a_{4\lambda}}{4}\boldsymbol{\sigma}:(\boldsymbol{\sigma}:(\boldsymbol{\lambda}_i^4-\boldsymbol{\lambda}_0^4):\boldsymbol{\sigma}):\boldsymbol{\sigma}\\
&\quad\leqslant 6\Delta G^\theta-A; \qquad (6)
\end{aligned}
$$

$\mathsf{M}_i\rightarrow\mathsf{M}_j$:

$$
\begin{aligned}
\frac{\partial^2 G(\boldsymbol{\sigma},\ \theta,\ \widehat{\eta_i})}{\partial\eta_j^2}=&-6\,\boldsymbol{\sigma}:(\boldsymbol{\varepsilon}_{tj}-\boldsymbol{\varepsilon}_{ti})-6\,\boldsymbol{\sigma}:(\boldsymbol{\varepsilon}_{\theta j}-\boldsymbol{\varepsilon}_{\theta i})\\
&-3\,\boldsymbol{\sigma}:(\boldsymbol{\lambda}_j-\boldsymbol{\lambda}_i):\boldsymbol{\sigma}-2(\boldsymbol{\sigma}:(\boldsymbol{\lambda}_j^3-\boldsymbol{\lambda}_i^3):\boldsymbol{\sigma}):\boldsymbol{\sigma}\\
&-\frac{3}{2}\boldsymbol{\sigma}:(\boldsymbol{\sigma}:(\boldsymbol{\lambda}_j^4-\boldsymbol{\lambda}_i^4):\boldsymbol{\sigma}):\boldsymbol{\sigma}+2\overline{A}\leqslant 0. \qquad (7)
\end{aligned}
$$

The transformation strain is equal to $-\partial G(\mathbf{0},\ \theta,\eta_i)/\partial\boldsymbol{\sigma}$ at zero thermal strain:

$$
\begin{aligned}
\boldsymbol{\varepsilon}_t=&\sum_{i=1}^{n}\boldsymbol{\varepsilon}_{ti}\varphi(a,\eta_i)-\frac{1}{2}\sum_{i=1}^{n-1}\sum_{j=i+1}^{n}\eta_i^2\eta_j^2[3(\eta_i^2\boldsymbol{\varepsilon}_{ti}+\eta_j^2\boldsymbol{\varepsilon}_{tj})\\
&+(a-3)(\eta_j^2\boldsymbol{\varepsilon}_{ti}+\eta_i^2\boldsymbol{\varepsilon}_{tj})]. \qquad (8)
\end{aligned}
$$

It is easily verified that $\boldsymbol{\varepsilon}_t$ satisfies all requirements: $\boldsymbol{\varepsilon}_t(\overline{0})=0$, $\boldsymbol{\varepsilon}_t(\widehat{\eta_i})=\boldsymbol{\varepsilon}_{ti}$, $\boldsymbol{\varepsilon}_t(\overline{\eta_i})=\boldsymbol{\varepsilon}_{ti}\varphi(a,\eta_i)$.

The thermodynamic equilibrium conditions $\partial G/\partial\eta_i=0$ ($i=1,\ldots,n$) have $n+1$ solutions corresponding to A and the M_i: $\eta=\overline{0}$ and $\eta=\widehat{\eta_i}$, $i=1,\ldots,n$. There are other solutions of $\partial G/\partial\eta_i=0$ that correspond to maxima or saddle points. In the case of a single variant, there is, in addition to the extrema at $\eta_1=0$ and $\eta_2=1$, an extremum at

$$
\eta_3=\sqrt{[A-a\,\boldsymbol{\sigma}:\boldsymbol{\varepsilon}_t+a_\theta\boldsymbol{\sigma}:(\boldsymbol{\varepsilon}_{\theta 0}-\boldsymbol{\varepsilon}_{\theta 1})+\Lambda]/3h},
$$

$$
\begin{aligned}
\Lambda:=&a_\lambda\boldsymbol{\sigma}:(\boldsymbol{\lambda}_0-\boldsymbol{\lambda}_1):\boldsymbol{\sigma}/2+a_{3\lambda}\boldsymbol{\sigma}:((\boldsymbol{\lambda}_0^3-\boldsymbol{\lambda}_1^3):\boldsymbol{\sigma}):\boldsymbol{\sigma}/3\\
&+a_{4\lambda}\boldsymbol{\sigma}:(\boldsymbol{\sigma}:((\lambda_0^4-\boldsymbol{\lambda}_1^4):\boldsymbol{\sigma})):\boldsymbol{\sigma}/4,
\end{aligned}
$$

$$
\begin{aligned}
h:=&A-4\Delta G^\theta-(a-4)\,\boldsymbol{\sigma}:\boldsymbol{\varepsilon}_t+(a_\theta-4)\,\boldsymbol{\sigma}:(\boldsymbol{\varepsilon}_{\theta 0}-\boldsymbol{\varepsilon}_{\theta 1})\\
&+(a_\lambda-4)\,\boldsymbol{\sigma}:(\boldsymbol{\lambda}_0-\boldsymbol{\lambda}_1):\boldsymbol{\sigma}/2\\
&+(a_{3\lambda}-4)\,\boldsymbol{\sigma}:((\boldsymbol{\lambda}_0^3-\boldsymbol{\lambda}_1^3):\boldsymbol{\sigma}):\boldsymbol{\sigma}/3\\
&+(a_{4\lambda}-4)\,\boldsymbol{\sigma}:(\boldsymbol{\sigma}:((\boldsymbol{\lambda}_0^4-\boldsymbol{\lambda}_1^4):\boldsymbol{\sigma})):\boldsymbol{\sigma}/4, \qquad (9)
\end{aligned}
$$

which corresponds to a maximum in G if $\eta_3<1$. The height of the activation barrier for the A→M PT can be calculated by substituting η_3 in Eq. (1):

$$\begin{aligned} G(\boldsymbol{\sigma},\theta,\eta_3)-G(\boldsymbol{\sigma},\theta,0)=&[2A-9\Delta G^{\theta}-(2a-9)\boldsymbol{\sigma}:\boldsymbol{\varepsilon}_t \\ &+(2a_{\theta}-9)\boldsymbol{\sigma}:(\boldsymbol{\varepsilon}_{\theta 0}-\boldsymbol{\varepsilon}_{\theta 1}) \\ &+(2a_{\lambda}-9)\boldsymbol{\sigma}:(\boldsymbol{\lambda}_0-\boldsymbol{\lambda}_1):\boldsymbol{\sigma}/2 \\ &+(2a_{3\lambda}-9)\boldsymbol{\sigma}:(\boldsymbol{\lambda}_0^3-\boldsymbol{\lambda}_1^3):\boldsymbol{\sigma}:\boldsymbol{\sigma}/3 \\ &+(2a_{4\lambda}-9)\boldsymbol{\sigma}:\boldsymbol{\sigma}:(\boldsymbol{\lambda}_0^4 \\ &-\boldsymbol{\lambda}_1^4):\boldsymbol{\sigma}:\boldsymbol{\sigma}/4]\eta_3^4/3. \end{aligned} \tag{10}$$

The activation barrier for the M→A PT is $G(\boldsymbol{\sigma},\theta,\eta_3)-G(\boldsymbol{\sigma},\theta,1)$, which can be obtained by adding $G(\boldsymbol{\sigma},\theta,0)-G(\boldsymbol{\sigma},\theta,1)=\boldsymbol{\sigma}:\boldsymbol{\varepsilon}_t-\Delta G^{\theta}$ to Eq. (10).

It is a good approximation over a modest range of temperatures to take ΔG^{θ} and A to be linear functions of the temperature,[1]

$$\Delta G^{\theta}=z(\theta-\theta_e),\quad A=A_0(\theta-\theta_c),\quad z>0,\quad A_0>0, \tag{11}$$

where θ_e is the equilibrium temperature for stress-free A and M, $-z$ is the jump in specific entropy at the equilibrium temperature, and θ_c is the critical temperature at which stress-free A loses its thermodynamic stability. Then

$$\begin{aligned} f=&A_0(\theta-\theta_c)\eta^2/2+[3z(\theta-\theta_e)-A_0(\theta-\theta_c)]\eta^4 \\ &+[A_0(\theta-\theta_c)-4z(\theta-\theta_e)]\eta^6/2. \end{aligned} \tag{12}$$

Designating the critical temperature at which stress-free M loses its thermodynamic stability as $\overline{\theta_c}$, one obtains $\overline{\theta_c}=\theta_c+6z(\theta_e-\theta_c)/(6z-A_0)$ with $A_0<6z$ from Eq. (6). The inequality $A_0<6z$ was assumed in the derivation of the equation for $\overline{\theta_c}$ and it follows from the evident inequalities $\overline{\theta_c}>\theta_e>\theta_c$ that it is not contradictory. For equal deviations of the critical temperatures from the equilibrium temperature one obtains $A_0=3z$ and further simplification of Eq. (12). For PT's that can be treated as one dimensional, i.e., $\boldsymbol{\sigma}:\boldsymbol{\varepsilon}_t=\sigma\varepsilon_t$, where σ and ε_t are scalar measures of stress and transformation strain,[1] Eq. (9) for η_3 provides us with the unstable equilibrium-stress–transformation-strain curve. Neglecting the differences between the compliances and thermal strain tensors of A and M we find

$$\sigma=\frac{3(A-4\Delta G^{\theta})\eta^2-A}{\varepsilon_t[3(a-4)\eta^2-a]}. \tag{13}$$

In the approximation (11), the σ-η curve depends linearly on temperature,

$$\sigma=\frac{3[A_0(\theta-\theta_c)-4z(\theta-\theta_e)]\eta^2-A_0(\theta-\theta_c)}{\varepsilon_t[3(a-4)\eta^2-a]}, \tag{14}$$

and for the stress hysteresis $H:=\sigma(\eta=0)-\sigma(\eta=1)$ one obtains

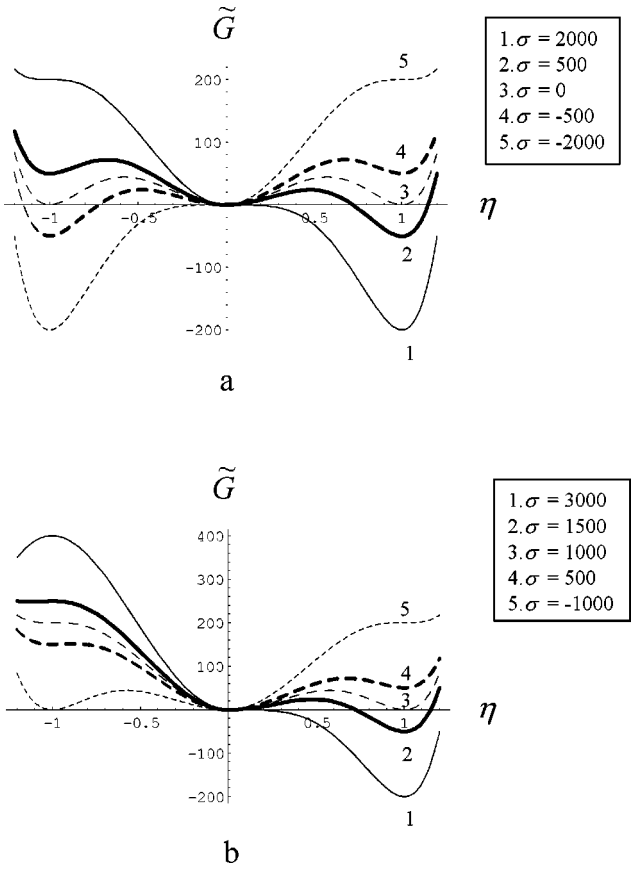

FIG. 1. $\tilde{G}(\eta)$ for equal deviations of the critical temperatures from the equilibrium temperature at various stresses for (a) $\theta=200$ K and (b) $\theta=250$ K. The same parameter values—namely $\varepsilon_t=0.1$, $a=3$, $\theta_c=100$ K, $\theta_e=200$ K, and $A_0=3$ MPa/K—were used for both plots.

$$H=\frac{6}{\varepsilon_t}\frac{(A_0-za)\theta+za\,\theta_e-A_0\theta_c}{a(6-a)}. \tag{15}$$

This expression for H is the same as for the 2-3-4-5 potential.[1] For $A_0>za$ ($A_0<za$) the hysteresis grows (decreases) with temperature and for $A_0=za$ it is independent of temperature.

The equation $\boldsymbol{\varepsilon}=-\partial G/\partial\boldsymbol{\sigma}$ gives the relation between strain and order parameters for any actual transformation path at constant $\boldsymbol{\sigma}$. Consider a single martensitic variant. In thermodynamic equilibrium, $\boldsymbol{\varepsilon}(\boldsymbol{\sigma},\eta)=-\partial G/\partial\boldsymbol{\sigma}$ and (9) for $\eta_3(\boldsymbol{\sigma})$ constitute a parametric relation between strain and order parameter with $\boldsymbol{\sigma}$ as the parameter. This $\boldsymbol{\varepsilon}$-η relation simplifies considerably in a linear elastic material for which Eq. (13) holds:

$$\varepsilon=\varepsilon_t\varphi(a,\eta)+\lambda\frac{3(A-4\Delta G^{\theta})\eta^2-A}{\varepsilon_t[3(a-4)\eta^2-a]}. \tag{16}$$

This equation is valid for $0\leqslant\eta\leqslant1$, i.e., for $\lambda A/(\varepsilon_t a)\leqslant\varepsilon\leqslant\varepsilon_t+\lambda(A-6\Delta G^{\theta})/[\varepsilon_t(a-6)]$.

In Fig. 1, we plot $\tilde{G}:=G+\frac{1}{2}\boldsymbol{\sigma}:\boldsymbol{\lambda}:\boldsymbol{\sigma}$ versus η for two temperatures and various stresses in the approximation (11) for $A_0=3z$, which corresponds to $\theta_e=(\theta_c+\overline{\theta_c})/2$; the exten-

sion to negative η will be considered in Sec. II B. In contrast to the 2-3-4-5 polynomial (see Fig. 6 in Ref. 1), the curvature (second derivative with respect to η) at the martensitic minimum is significantly larger than at the austenitic minimum. Indeed, the ratio $[\partial^2 G(1)/\partial\eta^2]/[\partial^2 G(0)/\partial\eta^2]$ for the 2-4-6 potential is 4 times greater than for the 2-3-4-5 polynomial. (Note that the curvatures of the A and M minima are the same for the 2-3-4-5 potential at thermodynamic equilibrium.) This difference is not related to differences in the elastic moduli or to the conditions for the loss of stability of homogeneous phases. This difference in curvature leads to significant differences between the profiles and energies of the critical martensitic nuclei for the 2-4-6 and 2-3-4 potentials (see Sec. V). It also leads to convergence of the solutions of the time-dependent Ginzburg-Landau equations to different equilibrium domain wall configurations for the same thermodynamic, initial, and boundary conditions, which will be described in detail elsewhere.

The stress-strain curve for the 2-4-6 polynomial is similar to that of the 2-3-4-5 polynomial, but there are differences; see Fig. 5 in Ref. 1. First, for $a=3$, σ is a linear function of η for the 2-3-4-5 polynomial, but σ is a nonlinear function of η for the 2-4-6 polynomial. The absolute value of the tangent elastic modulus at $\eta=1$ is much larger for the 2-4-6 polynomial than for the 2-3-4-5 polynomial, a consequence of the greater curvature of $G(\eta)$ at $\eta=1$.

B. Continuation of the 2-4-6 order parameters to negative values

Continuation of the order parameters to negative values requires that the term $C\eta_i^3\eta_j^3$ in F_{ij} be replaced by $C|\eta_i|^3|\eta_j|^3$. Then F_{ij} is invariant under $\eta_i\rightarrow-\eta_i$ or $\eta_j\rightarrow-\eta_j$ and spurious minima at $\pm\hat{\eta}_i\pm\hat{\eta}_j$, $\pm\hat{\eta}_i\pm\hat{\eta}_j\pm\hat{\eta}_k$, etc., can be eliminated by choosing $B\leqslant 0$ and $C>0$, as is the case for positive order parameters.

We start with the special case of martensitic variants with transformation strains that differ only in sign. This can be the case only if the transformation strain is purely deviatoric since the volumetric strains must be of the same sign. This condition is approximately met for the IPS variants in, for example, CuAlNi, CuZnGa, CuZn, CuAlZn, AgCd, and NiAl alloys.[8] These pairs of IPS variants with $\boldsymbol{\varepsilon}_t$ of opposite sign, M_+ and M_-, have equal elastic compliances. The thermal strain tensors will be treated below. Our 2-4-6 Landau potential, Eqs. (1)–(5), can be modified to describe transformations between A and n IPS variants and among n IPS variants with $n/2$ order parameters. A single order parameter is associated with M_+ and M_-; the variants are located at $\pm\hat{\eta}_i$ for some i. The modified form of the 2-4-6 potential is obtained by substituting $\boldsymbol{\varepsilon}_{ti}\mathrm{sgn}(\eta_i)$ for $\boldsymbol{\varepsilon}_{ti}$ and $n/2$ for n. The sign function $\mathrm{sgn}(\eta_i)=\eta_i/|\eta_i|$ is always multiplied by η_i^m, where $2\leqslant m\leqslant 6$. The second derivatives of the quadratic terms include terms of the form $2\,\mathrm{sgn}(\eta_i)$; therefore, $\partial^2 G/\partial\eta_i^2$ is discontinuous at the origin; G and $\partial G/\partial\eta_i$ are continuous at the origin.

Let us consider for simplicity η-independent elastic compliances. For just two IPS variants M_+ and M_-, the equilibrium condition $\partial G/\partial\eta=0$ gives, in addition to the roots $\eta_1=0$, $\eta_2=0$, and η_3 [see Eq. (9)], the negative roots

$$\eta_4=-1,\quad \eta_5=-\sqrt{\frac{a\boldsymbol{\sigma}:\boldsymbol{\varepsilon}_t+A}{3[(a-4)\boldsymbol{\sigma}:\boldsymbol{\varepsilon}_t-4\Delta G^\theta+A]}}. \tag{17}$$

The PT conditions, which follow from $\eta_3=0,1$ and $\eta_5=0$, -1, are

$$\mathsf{A}\rightarrow\mathsf{M}_+:\ \ \boldsymbol{\sigma}:\boldsymbol{\varepsilon}_t\geqslant\frac{A}{a};\ \ \mathsf{A}\rightarrow\mathsf{M}_-:\ \ \boldsymbol{\sigma}:\boldsymbol{\varepsilon}_t\leqslant-\frac{A}{a};$$

$$\mathsf{M}_+\rightarrow\mathsf{A}:\quad \boldsymbol{\sigma}:\boldsymbol{\varepsilon}_t\leqslant\frac{6\Delta G^\theta-A}{6-a};$$

$$\mathsf{M}_-\rightarrow\mathsf{A}:\quad \boldsymbol{\sigma}:\boldsymbol{\varepsilon}_t\geqslant-\frac{6\Delta G^\theta-A}{6-a}. \tag{18}$$

For $\Delta G^\theta>A(a-3)/3a$, the $\mathsf{M}_-\rightarrow\mathsf{A}$ PT occurs at smaller stresses than does the $\mathsf{A}\rightarrow\mathsf{M}_+$ PT; for $a=3$ this occurs at $\theta>\theta_e$. In this case M_- first transforms to A and then, after an increase in stress or a decrease in temperature, A transforms to M_+. In the opposite case, M_- transforms directly to M_+ because A is unstable.

A volume preserving IPS is a simple shear in direction $\boldsymbol{m}$ in the habit plane with normal $\boldsymbol{n}$, $\boldsymbol{\varepsilon}_t=\frac{1}{2}\gamma_t(\boldsymbol{mn}+\boldsymbol{nm})$, $\boldsymbol{\sigma}:\boldsymbol{\varepsilon}_t=\tau\gamma_t$, $\tau:=\boldsymbol{m}\cdot\boldsymbol{\sigma}\cdot\boldsymbol{n}$; here τ and γ_t are the shear stress and strain. The one-dimensional treatment presented in Ref. 1 is applicable.

In Fig. 1, the dependence of $\tilde{G}:=G+\frac{1}{2}\boldsymbol{\sigma}:\boldsymbol{\lambda}:\boldsymbol{\sigma}$ on η in the interval $[-1,1]$ is presented for two temperatures and various stresses for $A_0=3z$.

If part $\overline{\boldsymbol{\varepsilon}_{ti}}$ of the transformation strain is the same for the M_+ and M_- variants and another part $\overline{\overline{\boldsymbol{\varepsilon}_{ti}}}$ is of opposite sign, then both M_+ and M_- can be described by the single order parameter η_i upon substituting $\overline{\boldsymbol{\varepsilon}_{ti}}+\overline{\overline{\boldsymbol{\varepsilon}_{ti}}}\mathrm{sgn}(\eta_i)$ for $\boldsymbol{\varepsilon}_{ti}$ in Eqs. (1) and (5). For IPS, $\overline{\boldsymbol{\varepsilon}_{ti}}=\varepsilon\boldsymbol{n}_i\boldsymbol{n}_i$ and $\overline{\overline{\boldsymbol{\varepsilon}_{ti}}}=\frac{1}{2}\gamma_t(\boldsymbol{m}_i\boldsymbol{n}_i+\boldsymbol{n}_i\boldsymbol{m}_i)$, where ε, the strain normal to the habit plane, is equal to the volumetric strain. The thermal strain tensor may be similarly decomposed, $\boldsymbol{\varepsilon}_{\theta i}=\boldsymbol{\varepsilon}_{\theta i}^{dev}\mathrm{sgn}(\eta_i)+\boldsymbol{\varepsilon}_{\theta i}^{vol}$, where $\boldsymbol{\varepsilon}_{\theta i}^{dev}$ and $\boldsymbol{\varepsilon}_{\theta i}^{vol}$ are the deviatoric and volumetric parts of $\boldsymbol{\varepsilon}_{\theta i}$.

For the cubic-orthorhombic PT (e.g., Cu-Ni-Al and Au-Cd alloys) and the cubic-monoclinic-II PT (e.g., Cu-Zn-Al alloys), $\overline{\boldsymbol{\varepsilon}_{ti}}$ describes the diagonal components of $\boldsymbol{\varepsilon}_{ti}$ and $\overline{\overline{\boldsymbol{\varepsilon}_{ti}}}$ corresponds to the only shear component.[9] Three order parameters are needed to describe the six martensitic variants in the first case and six order parameters are required to describe the 12 variants in the second case. For the cubic-monoclinic-I PT (e.g., Ni-Ti alloys), $\overline{\boldsymbol{\varepsilon}_{ti}}$ is associated with one shear and the three diagonal components of $\boldsymbol{\varepsilon}_{ti}$, and $\overline{\overline{\boldsymbol{\varepsilon}_{ti}}}$ is associated with the other two shear components.

Note that a similar procedure for decreasing the number of degrees of freedom by a factor of 2 can be followed for

the 2-3-4-5 polynomial. In addition to substituting $\bar{\boldsymbol{\varepsilon}}_{ti} + \bar{\bar{\boldsymbol{\varepsilon}}}_{ti}\mathrm{sgn}(\eta_i)$ for $\boldsymbol{\varepsilon}_{ti}$, one needs to substitute $|\eta_i|$ for η_i for all odd powers of η_i.

III. POTENTIALS IN HYPERSPHERICAL COORDINATES

In the n-dimensional space of order parameters, all martensitic variants are located on the unit hypersphere; thus it is natural to construct Gibbs potentials using the hyperspherical order parameters r and ψ_k, $k=1,\ldots,n$. Here r is the radial coordinate in order-parameter space and $\pi\psi_k/2$ is the angle between the radius vector $\boldsymbol{r}$ and the η_k axis:

$$r=\left(\sum_{i=1}^{n}\eta_i^2\right)^{1/2}, \quad 0\leqslant\psi_k=\frac{2}{\pi}\cos^{-1}\frac{\eta_k}{r}\leqslant 1, \qquad \sum_{k=1}^{n}\cos^2\left(\frac{\pi}{2}\psi_k\right)=1. \tag{19}$$

The third equation is a constraint that can be eliminated by expressing G in terms of the η_k. New Gibbs potentials in r and ψ_k can be derived from our 2-3-4 and 2-4-6 potentials $G(r)$ for a single martensitic variant by allowing for ψ_k dependence in the transformation strain and including a term that introduces ψ_k-dependent barriers between all variants. We emphasize that the potentials in hyperspherical coordinates are not simply reparametrizations of the 2-3-4 and 2-4-6 potentials in Cartesian coordinates but rather new potentials with somewhat different physics. In contrast to the 2-3-4 and 2-4-6 potentials, the Gibbs potentials in r and the ψ_k have the following desirable features.

(i) They have no unphysical minima and have no constants that do not appear in the phase equilibrium and transformation conditions.

(ii) The paths of minimum free energy between variants are great circles on the unit hypersphere. Variant-variant transformations occur along these paths and can be parametrized by a single angle. This property of a potential in hyperspherical coordinates makes it possible to obtain an analytical kink solution of the time-independent Ginzburg-Landau equation that connects martensitic variants without passing through an austenitic minimum. Similar solutions cannot be obtained for the potentials in Cartesian order parameters.

A. Two martensitic variants

We now consider the case $n=2$ for η-independent elastic compliances and thermal strain tensor. A polar coordinate system can be used and all derivations are quite simple. Our Gibbs potential is given by

$$G(\boldsymbol{\sigma},\theta,r,\psi)=-\boldsymbol{\sigma}:\boldsymbol{\lambda}:\boldsymbol{\sigma}/2-\boldsymbol{\sigma}:[\boldsymbol{\varepsilon}_{t1}+(\boldsymbol{\varepsilon}_{t2}-\boldsymbol{\varepsilon}_{t1})P(\psi)]\varphi_p(r) + f_p(\theta,r)+\bar{A}Q(\psi)q_p(r), \tag{20}$$

where $p=4$ corresponds to the 2-3-4 polynomial, $p=6$ corresponds to the 2-4-6 polynomial, and $\psi\equiv\psi_1=1-\psi_2$. For $p=4$ we have[1]

$$\varphi_4(r)=ar^2+(4-2a)r^3+(a-3)r^4, \quad 0<a<6,$$

$$f_4(\theta,r)=Ar^2+(4\Delta G^\theta-2A)r^3+(A-3\Delta G^\theta)r^4, \tag{21}$$

and for $p=6$ see Eqs. (2) and (3) with r substituted for η_k. The functions P, Q, and q are to be determined. The requirement that G give the free energies of M_1 and M_2 at $\psi=0$ and $\psi=1$, respectively, implies the conditions

$$P(0)=0, \quad P(1)=1, \quad Q(0)=Q(1)=0. \tag{22}$$

Without loss of generality we assume $q(1)=1$. We require the radial derivative of $G(r,\psi)$ to vanish at the origin and at $r=1$ for $0\leqslant\psi\leqslant 1$:

$$\frac{\partial G(0,\psi)}{\partial r}=\frac{\partial G(1,\psi)}{\partial r}=0\Rightarrow\frac{dq(0)}{dr}=\frac{dq(1)}{dr}=0. \tag{23}$$

Similarly, the ψ derivative of $G(r,\psi)$ is forced to vanish at all r for $\psi=0,1$:

$$\frac{\partial G(r,0)}{\partial\psi}=\frac{\partial G(r,1)}{\partial\psi}=0\Rightarrow\frac{dP(0)}{d\psi}=\frac{dP(1)}{d\psi}=0, \qquad \frac{dQ(0)}{d\psi}=\frac{dQ(1)}{d\psi}=0. \tag{24}$$

These conditions include the equilibrium conditions $\partial G(\widehat{\eta}_j)/\partial\eta_i=0$ $(i,j=1,2)$ and also impose additional constraints on the form of the potential. Requiring that the inequality

$$\partial^2 G(1,\psi)/\partial\psi^2=-\boldsymbol{\sigma}:(\boldsymbol{\varepsilon}_{t2}-\boldsymbol{\varepsilon}_{t1})d^2P/d\psi^2+\bar{A}d^2Q/d\psi^2\leqslant 0 \tag{25}$$

for $\psi=0$ ($\psi=1$) coincide with Eq. (6) in part II (Ref. 2)—i.e., it give the same $\mathsf{M}_1\rightarrow\mathsf{M}_2$ ($\mathsf{M}_2\rightarrow\mathsf{M}_1$) PT criterion as Eq. (7) or (5) in (Ref. 2)—results in

$$\partial^2 P(0)/\partial\psi^2=-\partial^2 P(1)/\partial\psi^2=6, \qquad \partial^2 Q(0)/\partial\psi^2=\partial^2 Q(1)/\partial\psi^2=2. \tag{26}$$

We also require $\lim_{r\rightarrow 0}(q/\varphi)=\lim_{r\rightarrow 0}(q/r^2)=0$, which eliminates the barrier to the $\mathsf{M}_1\leftrightarrow\mathsf{M}_2$ PT in the vicinity of the origin. Otherwise, following $\mathsf{M}_{1,2}\rightarrow\mathsf{A}$, the A remembers the variant from which it came. Restricting our attention to 2-3-4 and 2-4-6 polynomials, we obtain the following functions which satisfy the above requirements:

$$Q=\psi^2(1-\psi)^2, \quad P=\psi^2(3-2\psi), \qquad q_4=4r^3-3r^4, \quad q_6=3r^4-2r^6. \tag{27}$$

The polynomials q, f, and φ must be of the same degree. If this were not the situation, then additional unphysical extrema might appear and an analytical study would not be possible. The polynomials in ψ can be used with both fourth- and sixth-degree polynomials in r. Note that Q can be written in the form $Q=\psi_1^2\psi_2^2$. For n martensitic variants, this generalizes to $Q=\psi_1^2\cdots\psi_n^2$; see next section.

Variant-variant transformations can be studied analytically by putting $r=1$ in the above equations. For example, a solution of the equation $\partial G(1,\psi)/\partial\psi=0$ is $\psi_3=1/2-(3S)/(2\overline{A})$ with $S:=\boldsymbol{\sigma}:(\boldsymbol{\varepsilon}_{t2}-\boldsymbol{\varepsilon}_{t1})$, which is the location of the barrier for the $\mathsf{M}_1\rightarrow\mathsf{M}_2$ PT. The corresponding activation barriers are

$$\begin{aligned} G(1,\psi_3)-G(1,0)&=(1-3S/\overline{A})^3(\overline{A}+S)/16,\\ G(1,\psi_3)-G(1,1)&=(1+3S/\overline{A})^3(\overline{A}-S)/16. \end{aligned} \tag{28}$$

A variant-variant kink solution of the time-independent Ginzburg-Landau equation for the $r=1$ potential will be obtained in Sec. V.

B. *n* martensitic variants

We assume η-independent elastic compliances and thermal strain. Equations (20) and (27) generalize to

$$G+\frac{1}{2}\boldsymbol{\sigma}:\boldsymbol{\lambda}:\boldsymbol{\sigma}=-\boldsymbol{\sigma}:\sum_{k=1}^{n}\boldsymbol{\varepsilon}_{tk}(1-3\psi_k^2+2\psi_k^3)\varphi_p(r) +f_p(\theta,r)+\overline{A}\prod_{k=1}^{n}\psi_k^2 q_p(r). \tag{29}$$

It is easy to check using $\psi_1+\psi_2=1$ that, for $n=2$, Eq. (29) reduces to Eq. (20) with P and Q given by Eq. (27).

We now verify the equilibrium conditions—namely, $\partial G/\partial\eta_i=0$—at the points $\overline{0}=(0,\ldots,0)$ and $\hat{\eta}_j$, $j=1,\ldots,n$, as well as the phase instability conditions:

$$\mathsf{M}_i\rightarrow\mathsf{A}\text{:}\quad \boldsymbol{\sigma}:\boldsymbol{\varepsilon}_{ti}\leqslant\frac{6\Delta G^\theta-A}{6-a}; \tag{30}$$

$$\mathsf{A}\rightarrow\mathsf{M}_i\text{:}\quad \boldsymbol{\sigma}:\boldsymbol{\varepsilon}_{ti}\geqslant\frac{A}{a}; \tag{31}$$

$$\mathsf{M}_j\rightarrow\mathsf{M}_i\text{:}\quad 3\boldsymbol{\sigma}:(\boldsymbol{\varepsilon}_{tj}-\boldsymbol{\varepsilon}_{ti})+\overline{\mathsf{A}}\leqslant 0. \tag{32}$$

These conditions are most easily verified by first expanding the potentials (29) around the points $\hat{\eta}_j$ and $\overline{0}$ to second order in the order parameters and then calculating the derivatives.

In the neighborhood of $\hat{\eta}_j$ the potential is

$$G=\Delta G^\theta-\frac{1}{2}\boldsymbol{\sigma}:\boldsymbol{\lambda}:\boldsymbol{\sigma}-\boldsymbol{\sigma}:\boldsymbol{\varepsilon}_{tj}+\frac{4}{\pi^2}\sum_{i\neq j}^{n}[3\boldsymbol{\sigma}:(\boldsymbol{\varepsilon}_{tj}-\boldsymbol{\varepsilon}_{ti})+\overline{A}]\eta_i^2 +\omega_p[(6-a)\boldsymbol{\sigma}:\boldsymbol{\varepsilon}_{tj}+A-6\Delta G^\theta](\eta_j-1)^2+O(\eta^3), \tag{33}$$

where $\omega_4=1$ and $\omega_6=2$. This always has an extremum at $\hat{\eta}_j$:

$$\frac{\partial G(\hat{\eta}_j)}{\partial\eta_i}=0,\quad i,j=1,\ldots,n. \tag{34}$$

The mixed derivatives $\partial^2 G/\partial\eta_i\partial\eta_j$ $(i\neq j)$ of Eq. (33) vanish at all $\hat{\eta}_k$. It follows that the conditions $\partial^2 G(\hat{\eta}_j)/\partial\eta_j^2\leqslant 0$ and $\partial^2 G(\hat{\eta}_j)/\partial\eta_i^2\leqslant 0$ are the conditions for $\mathsf{M}_j\rightarrow\mathsf{A}$ and $\mathsf{M}_j\rightarrow\mathsf{M}_i$, respectively. The $\mathsf{M}_j\rightarrow\mathsf{A}$ PT condition is given by

$$\frac{\partial^2 G(\hat{\eta}_j)}{\partial\eta_j^2}=2\omega_p[(6-a)\boldsymbol{\sigma}:\boldsymbol{\varepsilon}_{tj}+A-6\Delta G^\theta]\leqslant 0, \tag{35}$$

which coincides with Eq. (30). Similarly, the $\mathsf{M}_j\rightarrow\mathsf{M}_i$ PT condition is

$$\frac{\partial^2 G(\hat{\eta}_j)}{\partial\eta_i^2}=\frac{8}{\pi^2}[3\boldsymbol{\sigma}:(\boldsymbol{\varepsilon}_{tj}-\boldsymbol{\varepsilon}_{ti})+\overline{A}]\leqslant 0, \tag{36}$$

in agreement with Eq. (32).

In the neighborhood of the origin we have

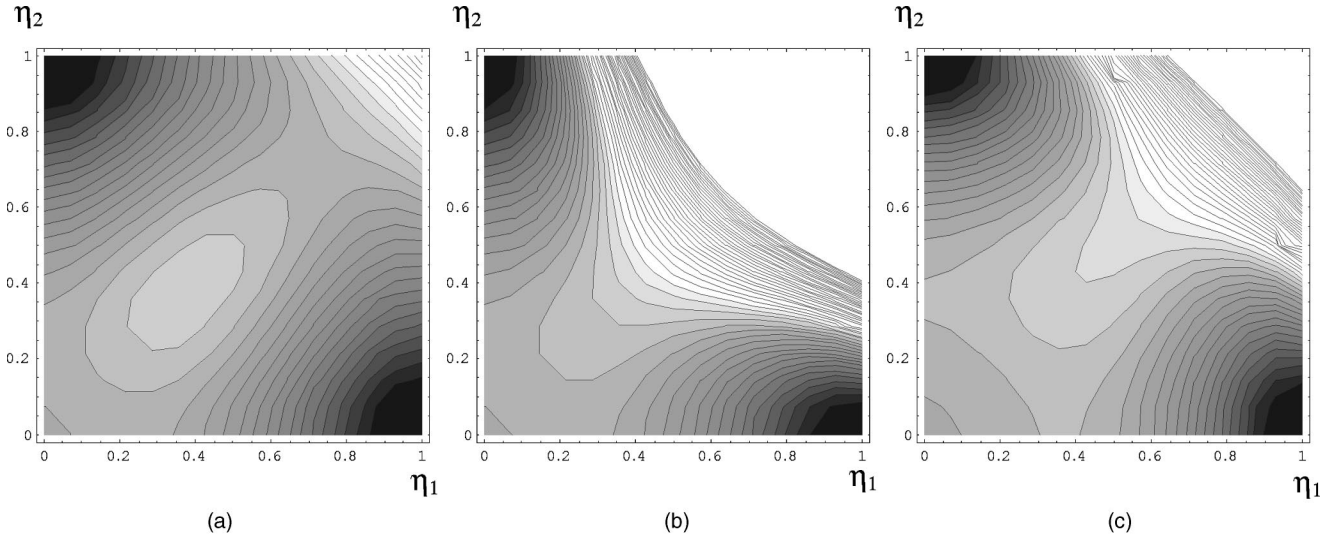

FIG. 2. Level curves of $\tilde{G}$ for NiAl at $\theta=0$ and normal stresses $\sigma_1=\sigma_2=\sigma_3=0$: (a) 2-3-4 polynomial in polar coordinates, (b) 2-3-4 polynomial in Cartesian coordinates, and (c) 2-4-6 polynomial in Cartesian coordinates.

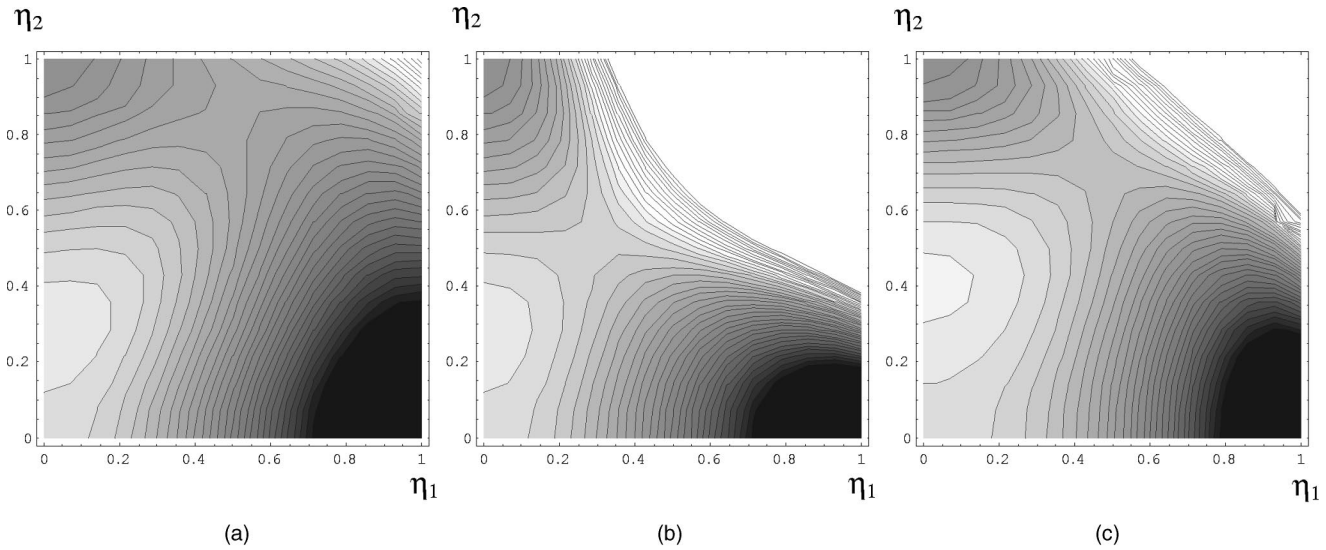

FIG. 3. Level curves of $\tilde{G}$ for NiAl at $\theta=0$ and normal stresses $\sigma_1=1000$, $\sigma_2=-1000$, $\sigma_3=-3000$: (a) 2-3-4 polynomial in polar coordinates, (b) 2-3-4 polynomial in Cartesian coordinates, and (c) 2-4-6 polynomial in Cartesian coordinates.

$$G=-\frac{1}{2}\boldsymbol{\sigma}:\boldsymbol{\lambda}:\boldsymbol{\sigma}+\omega_p^{-1}\left[-a\,\boldsymbol{\sigma}:\sum_{k=1}^{n}\boldsymbol{\varepsilon}_{tk}(1-3\psi_k^2+2\psi_k^3)+A\right]r^2 \tag{37}$$

$$\mathrm{A}\rightarrow\mathrm{M}_j\text{:}\quad \frac{\partial^2 G(r=0,\psi_j=0,\psi_i=1 \ \text{ for } \ i\neq j)}{\partial r^2}$$

$$=(2/\omega_p)(-a\,\boldsymbol{\sigma}:\boldsymbol{\varepsilon}_{tj}+A)\leqslant 0, \tag{38}$$

to second order in r. Obviously, G has an extremum at the origin for any stress or temperature. Unlike the mixed derivatives at the martensitic extrema, the mixed derivatives do not vanish at the origin, but as we shall see, the $\mathrm{A}\rightarrow\mathrm{M}_i$ PT is unaffected. The A instability must be determined from the first fulfillment of the condition $\partial^2 G/\partial r^2\leqslant 0$ in some radial direction. Since the minima of $\partial^2 G(\overline{0})/\partial r^2$ are along the coordinate axes, one gets

for the variant with the maximum value of $\boldsymbol{\sigma}:\boldsymbol{\varepsilon}_{tj}$, in agreement with Eq. (31).

Thus, the potential (29) in hyperspherical coordinates satisfies the equilibrium and PT conditions.

If $\overline{\boldsymbol{\varepsilon}}_{ti}$ is the same for M_+ and M_- variants and $\overline{\overline{\boldsymbol{\varepsilon}}}_{ti}$ is of opposite sign, then the number of order parameters is reduced by a factor of 2 by substituting $\overline{\boldsymbol{\varepsilon}}_{ti}+\overline{\overline{\boldsymbol{\varepsilon}}}_{ti}\mathrm{sgn}(\eta_i)$ for $\boldsymbol{\varepsilon}_{ti}$ in Eq. (29).

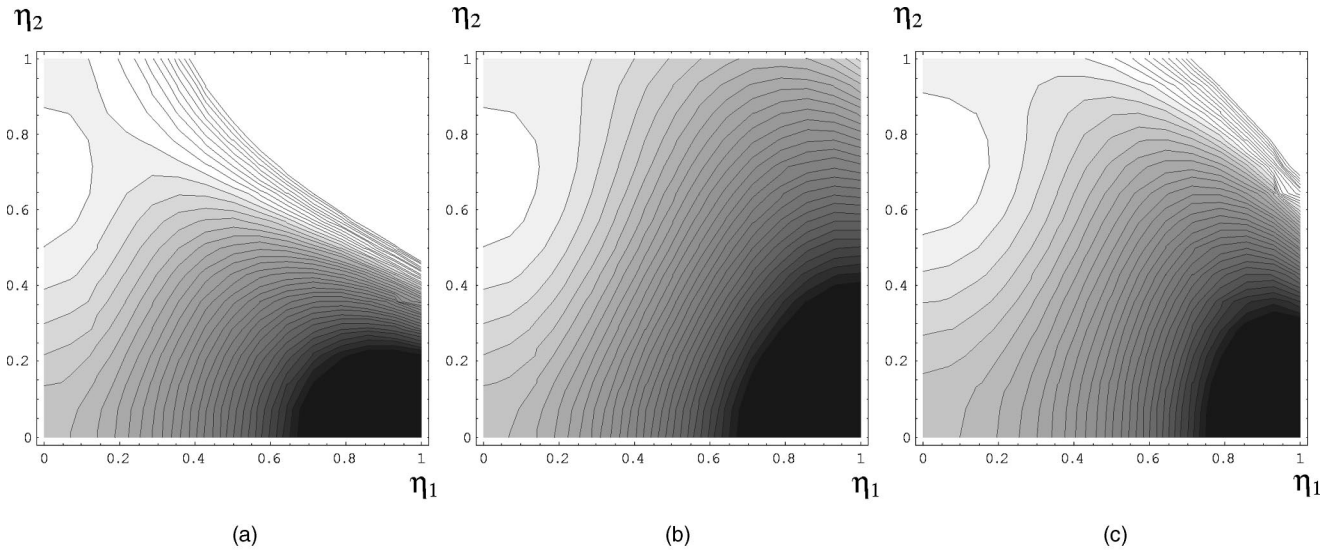

FIG. 4. Level curves of $\tilde{G}$ for NiAl at $\theta=0$ and normal stresses $\sigma_1=4051$, $\sigma_2=-2000$, $\sigma_3=-3000$: (a) 2-3-4 polynomial in polar coordinates, (b) 2-3-4 polynomial in Cartesian coordinates, and (c) 2-4-6 polynomial in Cartesian coordinates.

IV. COMPARISON OF POTENTIALS: THE NiAl CUBIC-TETRAGONAL PT

In part II (Ref. 2) we found all material parameters of the 2-3-4-5 potential for the cubic-to-tetragonal PT in NiAl. The relevant material constants for the 2-3-4-5 and polar 2-3-4 potentials are

$$\begin{gathered}\boldsymbol{\varepsilon}_{t1}=\{0.215;-0.078;-0.078\},\quad a=2.980,\\ \overline{A}=5320\ \text{MPa},\quad \theta_e=215\ \text{K},\\ A_0=4.40\ \text{MPa K}^{-1},\quad \theta_c=-183\ \text{K},\quad B=0,\\ D=500\ \text{MPa};\end{gathered}\tag{39}$$

the tensors $\boldsymbol{\varepsilon}_{t2}$ and $\boldsymbol{\varepsilon}_{t3}$ can be obtained by permutation of components. The constant D does not appear in the polar potential. We chose $C=-1000$ from the condition that at $\sigma=-7000$ MPa, which is far outside the region of stability of the martensite and consequently far beyond stresses of interest, $G(\sigma,0,1,1)\gg G(\sigma,0,1,0)$, and no unphysical minima exist. This ensures that the same is true at smaller compressive stresses or in tension.

Plots of $\tilde{G}(\boldsymbol{\sigma},\theta,\eta_1,\eta_2)=G(\boldsymbol{\sigma},\theta,\eta_1,\eta_2)+\frac{1}{2}\boldsymbol{\sigma}:\boldsymbol{\lambda}:\boldsymbol{\sigma}$ for PT's in NiAl for zero stress and two three-dimensional stress states at $\theta=0$ K for the 2-3-4-5, 2-4-6, and polar 2-3-4 potentials are shown in Figs. 2–4. The normal stresses on the faces of the crystal are denoted σ_i; all stresses are in MPa. We applied a large compressive stress σ_3 to suppress the appearance of the third variant. Growth of $\tilde{G}$ corresponds to variation from black to white. The driving force is orthogonal to the level curves. There are no unphysical minima present. This is particularly noteworthy for the polar 2-3-4 potential since it contains no constants that can be tuned to eliminate unphysical minima. We also checked this for the three-variant case by analyzing $\tilde{G}$ numerically.

For zero stresses (Fig. 2), both M variants are stable and A is metastable.

For $\sigma_1=-\sigma_2=1000$ (pure shear in the 1-2 plane), $\sigma_3=-3000$, M_1 is stable, M_2 is metastable, and A is unstable (Fig. 3). Because of a barrier between M_2 and A, A transforms to M_1 only.

For $\sigma_1=4051$, $\sigma_2=-2000$, and $\sigma_3=-3000$, M_1 is stable, and M_2 is unstable only in the direction of M_1 because the barrier between M_2 and A still exists (Fig. 4).

The energy variation along the coordinate axes is identical for the 2-3-4-5 potential and the polar 2-3-4 potential. The differences between these potentials are most pronounced for the stress-free case. Because the 2-4-6 potential has a much larger curvature at the M minimum than at the A minimum, there are significant differences in local values between the 2-4-6 and the other two potentials near the stable M minimum. As will be shown in Sec. V, such local differences result in different profiles for the critical M nuclei.

V. CRITICAL NUCLEI AND DIFFUSE INTERFACES

In this section we will obtain and interpret some spatially one-dimensional analytical solutions of the time-independent Ginzburg-Landau equations for the 2-3-4, 2-4-6, and r-ψ_k potentials. As was shown in Ref. 6, some two-dimensional problems for the cubic-rectangular PT can be treated as one dimensional, which is the case for our models as well. Our one-dimensional results on critical nuclei and diffuse interfaces hold for IPS variants—that is, for transformation strains of the form $\boldsymbol{\varepsilon}_t=\frac{1}{2}\gamma_t(\boldsymbol{mn}+\boldsymbol{nm})\operatorname{sgn}(\eta)+\varepsilon\boldsymbol{nn}$, where $-1\leqslant\eta\leqslant 1$ for the 2-4-6 potential and $0\leqslant\eta\leqslant 1$ for the 2-3-4 potential. The order parameter is a function of the coordinate x along the $\boldsymbol{n}$ axis. Despite the restriction to one spatial dimension, our solutions are valid for an arbitrary three-dimensional homogeneous stress tensor $\boldsymbol{\sigma}$ in a rectangular parallelepiped with corresponding homogeneous tractions at its faces. In order to impose the usual boundary condition on the order parameter [see Eq. (55)], the faces of the parallelepiped must be orthogonal and parallel to $\boldsymbol{n}$ (Fig. 5). In the following subsections the parallelepiped is actually infinite in the x direction.

A. Governing equations

We write the 2-4-6 and 2-3-4 potentials in terms of two parameters

$$\tilde{G}_6=s_1\eta^2[1-(4-P)\eta^2/2+(3-P)\eta^4/3]/2,\tag{40}$$

$$\tilde{G}_4=s_1\eta^2[1-(6-P)\eta/3+(4-P)\eta^2/4],\tag{41}$$

$$s_1:=A-a\,\boldsymbol{\sigma}:\boldsymbol{\varepsilon}_t,\quad s_2:=12(\Delta G^\theta-\boldsymbol{\sigma}:\boldsymbol{\varepsilon}_t),\quad P:=s_2/s_1.\tag{42}$$

Here and later the subscripts 4 and 6 refer to 2-3-4 or 2-4-6 potentials, respectively. We have

$$\begin{gathered}\partial G_6/\partial\eta=-s_1\eta(1-\eta^2)[(3-P)\eta^2-1],\\ \partial G_4/\partial\eta=s_1\eta(1-\eta)[2-(4-P)\eta];\\ \partial^2G_6(0)/\partial\eta^2=(1/2)\partial^2G_4(0)/\partial\eta^2=s_1,\\ \partial^2G_6(1)/\partial\eta^2=2\partial^2G_4(1)/\partial\eta^2=2s_1(2-P);\\ \eta_{63}=\sqrt{\frac{1}{3-P}},\quad \tilde{G}_6(\eta_{63})=\frac{s_1}{12}\frac{8-3P}{(P-3)^2};\\ \eta_{43}=\frac{2}{4-P},\quad \tilde{G}_4(\eta_{43})=\frac{4}{3}\frac{s_1(3-P)}{(4-P)^3}.\end{gathered}\tag{43}$$

Here η_{63} and η_{43} correspond to the maxima of $\tilde{G}$, as in Eq. (9).

For a single order parameter η that depends only on the coordinate x along the normal to the habit plane, the Ginzburg-Landau energy $G_{GL}=G+\nabla\eta\cdot\boldsymbol{\beta}\cdot\nabla\eta$ reduces to $G_{GL}=G+\beta(\partial\eta/\partial x)^2$, where the scalar β is a linear combination of components of the second-rank tensor $\boldsymbol{\beta}$ in the crystal coordinates. Thus, even for a highly anisotropic A

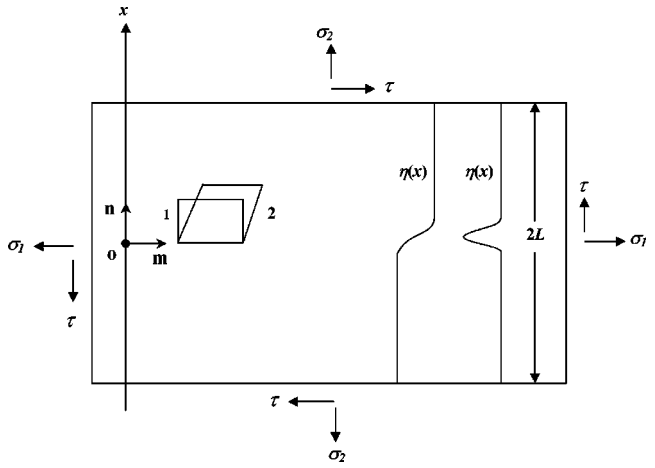

FIG. 5. Scheme for solution of the Landau-Ginzburg equation. $\eta(x)$ represents critical nuclei and kink solutions. The crystal lattice transforms from state 1 to 2 by invariant-plane strain.

lattice, the one-dimensional case under consideration requires only a single gradient parameter β. The Ginzburg-Landau energy G_{GL} leads to the time-dependent Ginzburg-Landau equation

$$\frac{\partial \eta}{\partial t} = -\lambda \frac{\delta G_{GL}}{\delta \eta} = -\lambda \left(\frac{\partial G}{\partial \eta} - 2\beta \frac{\partial^2 \eta}{\partial x^2} \right). \tag{44}$$

Here $\lambda > 0$ is the kinetic coefficient. We rescale variables to cast Eq. (44) in dimensionless form. The dimensionless potentials and order parameters are

$$g_6 = m_6 \tilde{G}_6 = B_6 \xi_6^2 - \xi_6^4 + \xi_6^6, \quad \xi_6 = k_6 \eta; \tag{45}$$

$$g_4 = m_4 \tilde{G}_4 = B_4 \xi_4^2 - \xi_4^3 + \xi_4^4, \quad \xi_4 = k_4 \eta. \tag{46}$$

The parameters are defined and related as follows:

$$\begin{aligned} B_6 &= \frac{4(3-P)}{3(4-P)^2}, \quad k_6 = \sqrt{\frac{2}{3}} \sqrt{\frac{3-P}{4-P}}, \\ m_6 &= \frac{16(3-P)^2}{9 s_1 (4-P)^3} = \frac{2 k_6^2 B_6}{s_1}; \\ B_4 &= \frac{9(4-P)}{4(6-P)^2}, \quad k_4 = \frac{3}{4} \frac{(4-P)}{(6-P)}, \\ m_4 &= \frac{81(4-P)^3}{64 s_1 (6-P)^4} = \frac{k_4^2 B_4}{s_1}. \end{aligned} \tag{47}$$

It is easy to check that k can be determined by the condition $dg/d\xi = 0$ at the martensitic minimum. Plots of $B(P)$, $k(P)$, and $s_1 m(P)$ in the region of coexistence of A and M ($P < 2$) for both potentials are presented in Fig. 6. We also define ξ_{61}, ξ_{62}, ξ_{41}, and ξ_{42}:

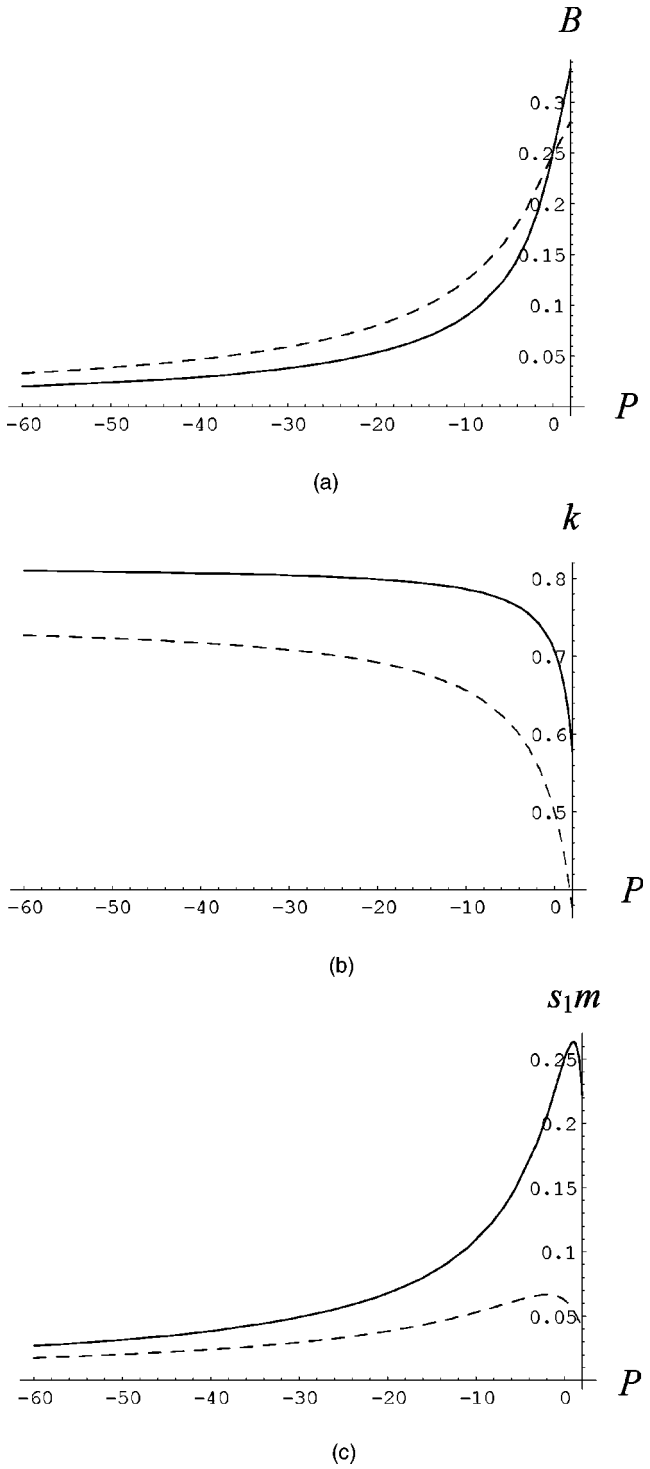

FIG. 6. Plots of (a) $B(P)$, (b) $k(P)$, and (c) $s_1 m(P)$. Solid (dashed) lines correspond to the 2-4-6 (2-3-4) potential.

$$\begin{aligned} g_6 &= \xi_6^2 (\xi_6^2 - \xi_{61}^2)(\xi_6^2 - \xi_{62}^2), \quad \xi_{61} = \sqrt{0.5(1 - \sqrt{1 - 4B_6})}, \\ \xi_{62} &= \sqrt{0.5(1 + \sqrt{1 - 4B_6})}; \\ g_4 &= \xi_4^2 (\xi_4 - \xi_{41})(\xi_4 - \xi_{42}), \quad \xi_{41} = 0.5(1 - \sqrt{1 - 4B_4}), \\ \xi_{42} &= 0.5(1 + \sqrt{1 - 4B_4}). \end{aligned} \tag{48}$$

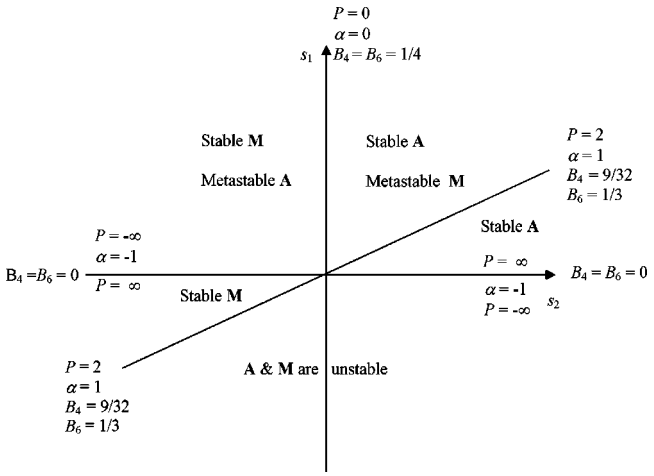

FIG. 7. Phase equilibrium and transformation diagrams in the s_1-s_2 plane for the 2-3-4 and 2-4-6 potentials.

We will analyze all results in terms of P, because it is the same for both polynomials, and in terms of $0 \leqslant B_4 \leqslant 9/32$ and $0 \leqslant B_6 \leqslant 1/3$, which vary over narrow ranges and allow more vivid comparisons. It is also convenient to use the parameter $\alpha := P/(4-P)$: $\alpha = 0$ for thermodynamic equilibrium, $\alpha = 1$ when M loses its stability, and $\alpha = -1$ when A loses its stability. Dimensionless order parameters and potentials are convenient for intermediate steps in calculations but our solutions of the time-independent Ginzburg-Landau equations are always presented in terms of the physical order parameter $\eta(x)$ for two reasons: first, there is no direct scaling between $\varphi(\xi)$ and $\varphi(\eta)$, and second, the dimensionless parameters for the two potentials—k_4 and k_6, for example—differ significantly for the same thermodynamic state.

Equilibrium and PT lines in the s_1-s_2 plane are shown in Fig. 7. The line $s_2 = 0$ ($P = 0$ and $B_4 = B_6 = 1/4$) for $s_1 \geqslant 0$ is the equilibrium line between A and M. For $s_2 > 0$ ($P > 0$ and $B > 1/4$) and $s_1 > 0$, A is stable (relative to M), and for $s_2 < 0$ ($P < 0$ and $0 < B < 1/4$) and $s_1 > 0$, M is stable. Martensite is also stable (relative to A) for $s_1 < 0$ and $P > 2$. The line $s_1 = 0$ for $s_2 \leqslant 0$ ($P = -\infty$ and $B = 0$) is the line of loss of stability of A; i.e., for $s_1 \leqslant 0$ and $s_2 \leqslant 0$ ($P \geqslant 0$), only M can exist, though not everywhere in this region. The line $P = 2$ ($B_4 = 9/32$, $B_6 = 1/3$) for $s_1 \geqslant 0$ is the line of loss of stability of M; i.e., for $P > 2$ and $s_1 \geqslant 0$, only A can exist. Consequently, both phases coexist in the sector $-\infty < P < 2$ ($0 < B_4 < 9/32$, $0 < B_6 < 1/3$) for $s_1 > 0$. The sector $-\infty < P < 2$ ($0 < B_4 < 9/32$, $0 < B_6 < 1/3$) for $s_1 < 0$ is an unphysical region because both M and A are unstable. In fact our potentials were designed to describe material behavior in the coexistence region and at instability lines. Our potentials are not applicable outside this region. Some of the above inequalities cannot be expressed in terms of B because B is a nonmonotonic function of P.

Austenite is stable relative to M in the wedge $s_1 > 0$, $P > 2$, but for $P > P_c^{\mathrm{A}}$, where $P_{6c}^{\mathrm{A}} = 8/3$ and $P_{4c}^{\mathrm{A}} = 3$, there is an artificial minimum more stable than A at $\eta > 1$ [see Eq. (43)]. For $s_1 < 0$ and $P > 2$, M is stable relative to A, but for $2 < P < P_c^{\mathrm{M}}$, where $P_{6c}^{\mathrm{M}} = 3$ and $P_{4c}^{\mathrm{M}} = 4$, a finite barrier at $\eta > 1$ separates the martensitic minimum from an infinitely deep potential well. For $s_1 < 0$ and $P < 2$, where A and M are unstable, there is an artificial minimum at $0 < \eta_3 < 1$.

These drawbacks do not affect the properties of the system in the coexistence region or along instability (PT) lines, but problems can arise when thermomechanical loading moves the point (s_1, s_2) too close to the unphysical wedge in the s_1-s_2 plane. If the initial phase is metastable, then rapid loading toward the unphysical wedge can result in a transformation to a spurious phase. On the other hand, if the rate of thermomechanical loading is sufficiently low, then the transition will be into the stable phase. In general, however, the rate will not be low enough to ensure transformation to the stable phase, but even if this is the case or if the initial phase is stable, the point (s_1, s_2) must not move too close to the unphysical wedge or else the small potential barrier separating the stable phase from the spurious phase will be surmounted by thermal fluctuations. These shortcomings in the potentials can be circumvented by modifying them outside the region of phase coexistence. The only requirements for such a modification are that it be continuous on the instability lines and that it have only one minimum in the region of M instability at $\eta = 0$ and a single minimum in the region of A instability at $\eta = 1$. So, for example, for $P > 2$ we can put

$$\begin{gathered}\tilde{G}_6 = s_1 \eta^2 (P - 1 - \eta^2 + \eta^4/3)/2, \\ \tilde{G}_4 = s_1 \eta^2 [P - 1 - (4/3)\eta + \eta^2/2], \quad s_1 > 0; \\ \tilde{G}_6 = s_1 (1 - s_1) P \eta^4 (\eta^2/3 - 1/2)/2, \\ \tilde{G}_4 = s_1 (1 - s_1) P \eta^2 (1/3 - \eta/4), \quad s_1 < 0.\end{gathered} \tag{49}$$

With such a modification, regions where only one phase exists can be correctly described in terms of P and B. For $P > 2$ ($0 < B_4 < 9/32$, $0 < B_6 < 1/3$), only A exists for $s_1 > 0$ and only M exists for $s_1 < 0$.

As an alternative to modifying the potential, the order parameters can be constrained in numerical simulations to the interval $[0,1]$ or $[-1,1]$ for the extended 2-4-6 potential. In other words, reflective boundary conditions can be imposed at the ends of these intervals.

Introducing new spatial and time variables by the equations

$$y_6 = \frac{k_6}{\sqrt{\beta m_6}} x = \sqrt{\frac{s_1}{2\beta B_6}} x = \frac{\sqrt{6}}{4} \sqrt{\frac{s_1}{\beta}} \frac{4-P}{\sqrt{3-P}} x, \quad z_6 = \frac{\lambda k_6^2}{m_6} t; \tag{50}$$

$$y_4 = \frac{k_4}{\sqrt{\beta m_4}} x = \sqrt{\frac{s_1}{\beta B_4}} x = \frac{2}{3} \sqrt{\frac{s_1}{\beta}} \frac{6-P}{\sqrt{4-P}} x, \quad z_4 = \frac{\lambda k_4^2}{m_4} t,$$

we obtain the dimensionless form of the Ginzburg-Landau equation

$$\frac{\partial \xi}{\partial z} = -\left(\frac{\partial g}{\partial \xi} - 2 \frac{\partial^2 \xi}{\partial y^2} \right). \tag{51}$$

Henceforth we consider only time independent solutions—i.e., $\partial \xi / \partial z = 0$. The resulting equation $2 d^2 \xi / dy^2 = dg/d\xi$ is

the equation of motion of a material point with mass equal to 2 in the potential field $-g(\xi)$. An energy integral reads

$$d\xi/dy=\sqrt{g-g_0}, \tag{52}$$

where g_0 is the integration constant. At points where $d\xi/dy=0$, e.g., at the center of a nucleus, $g=g_0$. Designating

$$g^*_{GL}=g_{GL}-g_0=g-g_0+(d\xi/dy)^2 \tag{53}$$

and taking into account Eq. (52), one finds that the contributions to g^*_{GL} from $g-g_0$ and the gradient of the order parameter ξ are the same, hence $g^*_{GL}=2(g-g_0)$. Generally, Eq. (52) has periodic solutions with n diffuse interfaces. The total energy per unit area of n diffuse interfaces is given by

$$e:=\int_{-l}^{l} g^*_{GL}dy=2n\int \sqrt{g-g_0}d\xi, \tag{54}$$

where $l:=\sqrt{s_1/(\beta B)}L$, $2L$ is the length of a parallelepiped in the x direction, and the integration limits of the second integral depend on the type of interface. The energy e is finite even for an infinite slab. The total energy of the system is infinite for an infinite parallelepiped in the case $g_0\neq 0$.

Falk[5] found periodic solutions for n domain walls in finite regions, but claims that the separation between domain walls must be infinite in an infinite region. However, all of his finite-l solutions depend on l only through the combination l/n. Consequently, the finite-l solutions can be used for $l\to\infty$ provided $n\to\infty$, keeping the ratio l/n, the distance between the domain walls, finite.

Imposing the usual boundary conditions at the ends of the slab

$$d\xi(-l)/dy=d\xi(l)/dy=0, \tag{55}$$

one obtains

$$g(-l)=g(l)=g_0. \tag{56}$$

Using Eq. (45), one derives

$$y_4(\xi_4)=\int \frac{d\xi_4}{\sqrt{B_4\xi_4^2-\xi_4^3+\xi_4^4-g_{40}}},$$
$$y_6(\xi_6)=\int \frac{d\xi_6}{\sqrt{B_6\xi_6^2-\xi_6^4+\xi_6^6-g_{60}}}. \tag{57}$$

Despite the significant differences between our theory and Falk's[5] and completely different variables and parameters, Eq. $(57)_2$ is of the same form as Eq. (14) in Ref. 5. This means that we can use all of Falk's formal periodic analytical solutions and analyze them in terms of our governing parameters for the 2-4-6 potential. The same procedure can be followed for the calculation of the total energy of the system.

B. Critical martensitic nucleus: M soliton in A

Let us start with the case when A exists as $x\to\pm\infty$, hence $g_0=0$. The solutions below are valid in the region of stability of M and metastability of A, i.e., $s_1>0$ and $P\leqslant 0$ ($0\leqslant B\leqslant 1/4$). One has

$$\xi_4^{\mathrm{M}}(y_4)=\frac{\xi_{41}}{1+\left(1-\frac{\xi_{41}}{\xi_{42}}\right)\sinh^2[\sqrt{B_4}(y_4-y_{04})/2]},$$
$$\xi_6^{\mathrm{M}}(y_6)=\frac{\xi_{61}}{\sqrt{1+\left(1-\frac{\xi_{61}^2}{\xi_{62}^2}\right)\sinh^2[\sqrt{B_6}(y_6-y_{06})]}}, \tag{58}$$

$$\eta_4^{\mathrm{M}}(x)=\frac{\xi_4\left(\sqrt{\frac{s_1}{\beta B_4}}x\right)}{k_4}$$
$$=6\{6-P+\sqrt{P^2-3P}\cosh[\sqrt{s_1/\beta}(x-x_0)]\}^{-1},$$
$$\eta_6^{\mathrm{M}}(x)=\frac{\xi_6\left(\sqrt{\frac{s_1}{2\beta B_6}}x\right)}{k_6} \tag{59}$$
$$=2\{4-P+\sqrt{P^2-8P/3}\cosh[\sqrt{2s_1/\beta}(x-x_0)]\}^{-1/2}.$$

The energies are given by

$$e_4^{\mathrm{M}}=(3-8B_4)\sqrt{B_4}/6+(B_4-1/4)\ln\frac{1+2\sqrt{B_4}}{\sqrt{1-4B_4}},$$
$$e_6^{\mathrm{M}}=\sqrt{B_6}/2+(B_6-1/4)\ln\frac{1+2\sqrt{B_6}}{\sqrt{1-4B_6}}, \tag{60}$$
$$E_4^{\mathrm{M}}=\frac{1}{k_4^2}\sqrt{\frac{\beta s_1}{B_4}}e_4^{\mathrm{M}}=\frac{32}{27}\frac{(6-P)^3}{(4-P)^{5/2}}\sqrt{\beta s_1}e_4^{\mathrm{M}},$$
$$E_6^{\mathrm{M}}=\frac{1}{k_6^2}\sqrt{\frac{\beta s_1}{2B_6}}e_6^{\mathrm{M}}=\frac{3\sqrt{6}}{8}\frac{(4-P)^2}{(3-P)^{3/2}}\sqrt{\beta s_1}e_6^{\mathrm{M}}.$$

The solution $\xi_6^{\mathrm{M}}(y_6)$ formally coincides with Falk's solution.[5] Falk did not provide a physical interpretation of his solution, but we do so here. At first sight, the solution (58) looks contradictory: the smaller B (more negative P) and the greater the stability of M, the smaller the magnitude of the order parameter of the M nucleus. This apparent contradiction disappears if we interpret the above solution as a *critical martensitic nucleus in austenite*. We verified by numerically solving the Ginzburg-Landau equation (51) that this solution corresponds to unstable thermodynamic equilibrium. An initial profile slightly larger (or smaller) than

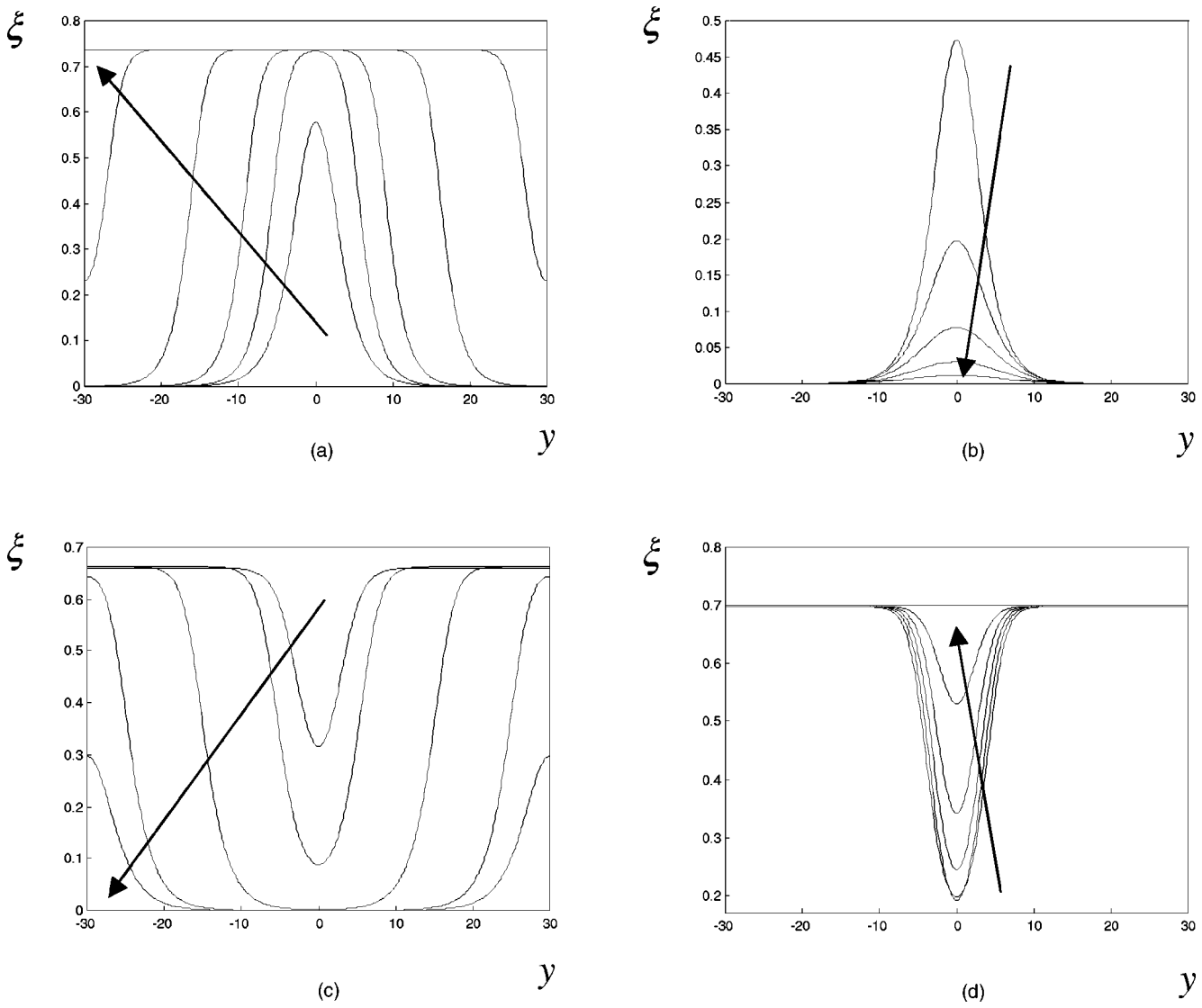

FIG. 8. (a) Growth of a supercritical M nucleus ($B=0.2$, $w=1.1$). (b) Disappearance of a subcritical M nucleus ($B=0.24$, $w=0.9$). (c) Growth of a supercritical A nucleus ($B=0.3$, $w=1.1$). (d) Disappearance of a subcritical A nucleus ($B=0.26$, $w=0.9$). All plots are for the 2-4-6 potential.

$\xi_6^{\mathrm{M}}(y_6)$ converges to M (or A) everywhere; see Fig. 8. The smaller B, the smaller the size and energy [see Eq. (60)] of the critical nucleus. Numerical solution of the Ginzburg-Landau equation for the 2-3-4 potential confirms that $\xi_4^{\mathrm{M}}(y_4)$ is also a critical M nucleus.

Only for thermodynamic equilibrium, $P=0$ or $B=1/4$, does the magnitude of the order parameter $\xi_{41}=\xi_{61}^2=1/2$ correspond to complete M ($\eta=1$); otherwise, it is smaller. Note that for homogeneous stresses and temperature, there is no solution for a stable M nucleus that grows with an increase in the thermodynamic driving force for the A$\rightarrow$M PT.

Let us designate the solution of the stationary Ginzburg-Landau equation as ξ_s. We will consider the 2-4-6 potential; the derivations and results for the 2-3-4 polynomial are similar. We can estimate $\partial\xi/\partial z$ at the instant when the nucleus $w\xi_s$ appears from Eq. (51); w is a constant multiplicative factor:

$$\frac{\partial\xi}{\partial z}=-\left(\frac{\partial g(w\xi_s)}{\partial\xi}-2w\frac{\partial^2\xi_s}{\partial y^2}\right)$$
$$=-\frac{\partial g(w\xi_s)}{\partial\xi}+w\frac{\partial g(\xi_s)}{\partial\xi}$$
$$=2\xi_s^3w(w^2-1)[2-3\xi_s^2(1+w^2)]. \qquad (61)$$

Consider a supercritical nucleus, i.e., $w>1$, for which we expect $\partial\xi/\partial z>0$. However, this is true only when $\xi_{s,max}$ satisfies $\xi_{s,max}^2<2/[3(1+w^2)]<1/3$, which is the case for $B<2/9$. For a small thermodynamic driving force $2/9\leqslant B\leqslant 1/4$, the inequality $\xi_1^2<2/[3(1+w^2)]$ is violated in the central part of the nucleus. Consequently, the magnitude of ξ initially decreases near the center of the nucleus while it grows in the rest of the nucleus. After a short initial stage, growth occurs throughout the nucleus.

For a subcritical nucleus, $w<1$, $\partial\xi/\partial z<0$ if the same inequality is satisfied. In this case, the central region of the nucleus grows during a brief initial stage, after which ξ decreases throughout the nucleus until it disappears.

The above analytical estimates provide important insights into the behavior of the nuclei but, of course, detailed, quantitative results on the growth or shrinkage of the nuclei can only be obtained from numerical simulations, for example, Fig. 8.

As was mentioned, for the 2-4-6 potential we can use Falk's periodic, multinuclei solutions for a finite region[5] the energy of such solutions (the activation energy for nucleation) is roughly proportional to the number of nuclei $n/2$. However, the physical interpretation of multinuclei solutions is unclear. Is this a stable solution or an unstable one? If it is a metastable configuration, can it be reached under some dynamic process and how high is the energy barrier that separates it from a lower-energy state with a smaller number of nuclei or from a complete M state? These problems will be studied elsewhere.

The amplitudes of the physical order parameters of the critical M nuclei are

$$\eta_{41}=\frac{\xi_{41}}{k_4}=\frac{4(1-\sqrt{1-4B_4})}{3+\sqrt{9-32B_4}},$$
$$\eta_{61}=\frac{\xi_{61}}{k_6}=\sqrt{\frac{3}{2}}\frac{1-\sqrt{1-4B_6}}{1+\sqrt{1-3B_6}}. \tag{62}$$

From now on, a subscript ''1'' on an order parameter will indicate the amplitude of that order parameter. The functions η_1 and $\varphi(\eta_1)$ vs B are shown in Fig. 9. The amplitude η_{61} is significantly larger than η_{41} except at the end points $B=0$ and $B=1/4$. Note that $d\eta_1/dB$ is infinite at the end points for the 2-4-6 potential and only at $B=1/4$ for the 2-3-4 polynomial.

Figure 10 shows $E^{\mathrm{M}}/\sqrt{\beta s_1}$ as a function of $\alpha=P/(4-P)$. The energy of the 2-3-4 critical M nucleus is smaller than the energy of the critical M nucleus for the 2-4-6 potential. The activation energy in thermodynamic equilibrium ($\alpha=0$) is finite, in contrast to the infinite energy of a classical nucleus with a sharp interface. When A loses its stability, $E_6^{\mathrm{M}}=E_4^{\mathrm{M}}=0$, while the activation energy is finite in classical nucleation theory.

The profiles $\eta(\sqrt{s_1/\beta}x,P)$ and $\varphi(\sqrt{s_1/\beta}x,P)$ of the critical nuclei are shown in Fig. 11 for various P and B. The φ profiles are essentially strain profiles because $\varepsilon_t\varphi[\eta(x)]$ is the transformation strain. The φ and η profiles are quite different, especially for small η and $1-\eta$ where the strongest nonlinearities of the function φ are located. The φ profiles are narrower than the η profiles. For $P=-1$ the 2-4-6 and 2-3-4 nuclei are almost indistinguishable. At larger P the 2-4-6 and 2-3-4 nuclei have the same amplitudes but the 2-3-4 nucleus is wider. At smaller P, $\varphi_6[\eta_6(x)]$ is significantly greater than $\varphi_4[\eta_4(x)]$ everywhere. When $P\to 0$, the entire region is martensite.

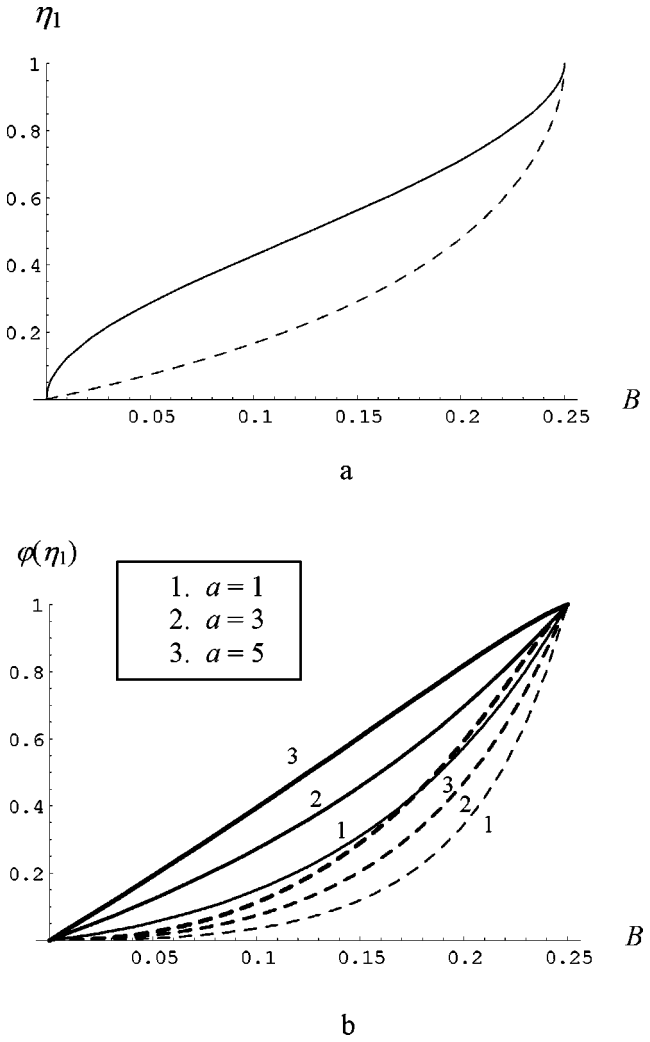

FIG. 9. The amplitudes of the critical M nuclei vs B: (a) the function $\eta_1(B)$, (b) the functions $\varphi[\eta_1(B)]$ for several a. Solid (dashed) lines correspond to the 2-4-6 (2-3-4) potential.

The effective width W of the nucleus can be defined as $W=2u(\infty)/\varepsilon\varphi(\eta_1)$, where $u(\infty)$ is the displacement at infinity and ε is the volumetric strain. Thus a nucleus of width W with a sharp interface and constant volumetric strain $\varepsilon\varphi(\eta_1)$ produces the same displacement increment as the critical nucleus. The displacement at infinity due to volumetric strain can be calculated by integrating

$$\varepsilon\varphi[\eta(x)]=\frac{du}{dx}, \tag{63}$$

where $u(0)=0$. The total displacement contains an additional contribution due to constant elastic strain, $u_e=2l\boldsymbol{nn}:\boldsymbol{\lambda}:\boldsymbol{\sigma}$, which we neglect here. The effective widths of the nuclei are

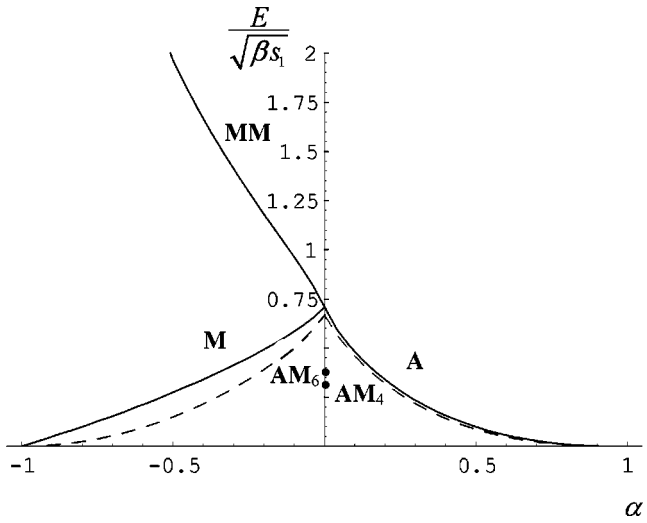

FIG. 10. The energy $E/\sqrt{\beta s_1}$ vs $\alpha=P/(4-P)$ for the critical M nuclei, the critical A nuclei, the A-M interfaces for the 2-3-4 (AM_4) and 2-4-6 (AM_6) potentials, and the M-M interface for the 2-4-6 potential. Solid (dashed) lines correspond to the 2-4-6 (2-3-4) potential.

$$W_6^{\mathrm{M}}(P)=\frac{3}{8(3-P)^2\varphi_6(\eta_{61})}\sqrt{\frac{\beta}{2s_1}}\left\{\frac{1}{6}\sqrt{\frac{3}{3-P}}\tanh^{-1}\left(\frac{1}{4}\sqrt{\frac{3}{3-P}}(4-P-\sqrt{P^2-8P/3})\right)\right.$$
$$\left.\times[576-24(a+14)P+(11a+36)P^2]+12a+(12-7a)P\right\},$$
$$W_4^{\mathrm{M}}(P)=\frac{8}{9(4-P)^3\varphi_4(\eta_{41})}\sqrt{\frac{\beta}{s_1}}\left\{\frac{2}{3\sqrt{4-P}}\tanh^{-1}\left(\frac{6-P-\sqrt{P^2-3P}}{3\sqrt{4-P}}\right)\right. \tag{64}$$
$$\left.\times[864-36(a+15)P+18(a+5)P^2-(a+6)P^3]-24(3-a)+12(6-a)P-(a+6)P^2\right\}.$$

We define the interface thickness as

$$\Delta^{\mathrm{M}}:=\frac{\varphi(\eta_1)}{|d\varphi[\eta(x_m)]/dx|}, \tag{65}$$

where x_m corresponds to the maximum of the derivative $d\eta(x)/dx$. The ideal definition would be $\Delta^{\mathrm{M}}:=\varphi(\eta_1)/|d\varphi[\eta(x)]/dx|_{max}$ but this cannot be analyzed analytically. The interface thicknesses are

$$\Delta_4^{\mathrm{M}}=\frac{(3+I_4)^5[12B_4-(I_4-3)(J_4-1)]}{96\sqrt{B_4}(1+J_4)^2(1+I_4+2J_4)[3(3+I_4)-32B_4]\sqrt{(I_4-3)(1+J_4)+12B_4}}\sqrt{\frac{\beta}{s_1}},$$
$$\Delta_6^{\mathrm{M}}=\frac{(1+J_6)^4[4B_6-(I_6-1)(J_6-1)]}{2\sqrt{B_6}(1+I_6)(1+I_6+2J_6)(1+J_6-3B_6)\sqrt{(1+I_6)(J_6-1)+4B_6}}\sqrt{\frac{\beta}{s_1}}, \tag{66}$$
$$I_4:=\sqrt{9-32B_4},\quad J_4:=\sqrt{1-4B_4},\quad I_6:=\sqrt{1-4B_6},\quad J_6:=\sqrt{1-3B_6}.$$

The dimensionless width $W^{\mathrm{M}}\sqrt{s_1/\beta}$ and dimensionless thickness $\Delta^{\mathrm{M}}\sqrt{s_1/\beta}$ are plotted as functions of B in Fig. 12. The width $W^{\mathrm{M}}\sqrt{s_1/\beta}$ tends to infinity for both potentials as the PT equilibrium line ($B=1/4$, $P=0$) is approached, while the interface thickness $\Delta^{\mathrm{M}}\sqrt{s_1/\beta}$ remains finite. As $B\to 0$ ($s_1\to 0$), $W^{\mathrm{M}}\sqrt{s_1/\beta}$ and $\Delta^{\mathrm{M}}\sqrt{s_1/\beta}$ go to finite values; therefore, W^{M} and Δ^{M} tend to infinity. Excluding the neighborhood of $B=1/4$, both parameters are of comparable magnitude; the interface is sharp only near thermodynamic equilibrium. The width of the nucleus is larger for the 2-4-6

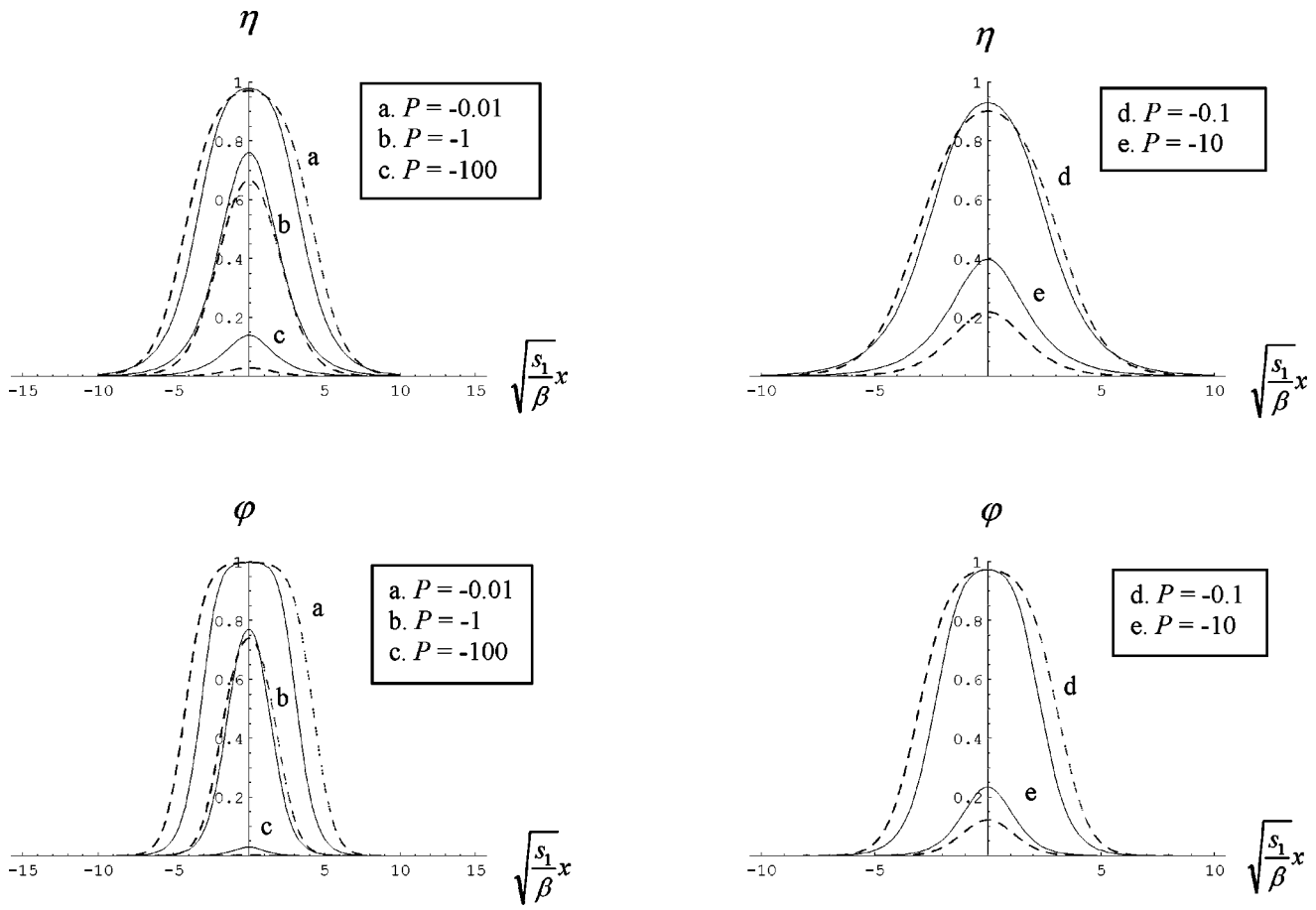

FIG. 11. Profiles of critical martensitic nuclei for various P and $a=2.98$. Solid (dashed) lines are for the 2-4-6 (2-3-4) potential.

potential than for the 2-3-4 potential. The interface thickness is significantly larger for the 2-3-4 potential for $B>0.17$ and almost the same for both potentials for smaller B.

The interface thicknesses Δ_4^{M} and Δ_6^{M} are given to within 0.4% by the cubic polynomial approximations

$$\Delta_4^{\mathsf{M}}=(1.942+1.779B_4-12.80B_4^2+68.56B_4^3)\sqrt{\frac{\beta}{s_1}},$$
$$\Delta_6^{\mathsf{M}}=(2.000+0.732B_6+0.381B_6^2+10.66B_6^3)\sqrt{\frac{\beta}{s_1}}. \tag{67}$$

The effective surface energy of a nucleus is defined in Ref. 7 as $\Gamma^{\mathsf{M}}:=[E^{\mathsf{M}}-G(\eta_1)W]/2$, so $G(\eta_1)W$ is the effective bulk energy of the nucleus. However, $G(\eta_1)=0$ by definition of η_1 [see Eq. (52) for $d\xi/dy=0$ and $g_0=0$]; i.e., the energy of the nucleus is localized at its surface according to this definition. For our theory, a better definition is $\Gamma^{\mathsf{M}}:=\{E^{\mathsf{M}}-G[\varphi(\eta_1)]W\}/2$ since $G[\varphi(\eta_1)]\neq 0$.

C. Kink solutions: A-M diffuse interfaces

We consider the case where the phase is A as $x\to-\infty$ and M as $x\to+\infty$. Then, $g(-\infty)=g(\mathsf{A})=g0=0$ and $g(+\infty)=g(\mathsf{M})=g_0$, i.e., $g(\mathsf{A})=g(\mathsf{M})=0$, which is the case when A and M are in thermodynamic equilibrium: $s_2=P=0$, $B=1/4$, $\xi_{41}=\xi_{42}=\xi_{61}^2=\xi_{62}^2=1/2$, $g_6=\xi_6^2(\xi_6^2-1/2)^2$, $g_4=\xi_4^2(\xi_4-1/2)^2$. The solutions of Eq. (52) read

$$\xi_4^{\mathsf{AM}}(y_4)=[2(1+e^{-(y_4-y_{04})/2})]^{-1},$$
$$\xi_6^{\mathsf{AM}}(y_6)=[2(1+e^{-(y_6-y_{06})})]^{-1/2},\ e_6^{\mathsf{AM}}=3e_4^{\mathsf{AM}}=1/8; \tag{68}$$
$$\eta_4^{\mathsf{AM}}(x)=\{1+\exp[-\sqrt{s_1/\beta}(x-x_0)]\}^{-1},$$
$$\eta_6^{\mathsf{AM}}(x)=\{1+\exp[-\sqrt{2s_1/\beta}(x-x_0)]\}^{-1/2}.$$

The solution $\eta_4^{\mathsf{AM}}(x)$ is symmetric around $x=x_0$ but η_6^{AM} is not (see Fig. 13) because the A and M minima of the 2-4-6 potential have different curvatures [note, however, that $(\eta_6^{\mathsf{AM}})^2$ is symmetric around $x=x_0$]. In Fig. 13 we used $x_{04}=0$ and $x_{06}=-\ln 3$ so that $\eta_6(0)=\eta_4(0)=1/2$. The strain profiles $\varphi_4[\eta(x)]$ and $\varphi_6[\eta(x)]$ are very close and exhibit smaller interface thicknesses than the $\eta(x)$ profiles.

A and M are in thermodynamic equilibrium, thus $s_2=P=0$, and consequently, $\Delta G^{\theta}=\boldsymbol{\sigma}:\boldsymbol{\varepsilon}_t$, $B=1/4$, and $k_6^2=1/2$. The interface energy densities are

$$E_6^{\mathrm{AM}}=\frac{3}{4}\sqrt{2}E_4^{\mathrm{AM}}=\frac{\sqrt{2\beta s_1}}{4}=\frac{\sqrt{2\beta}}{4}\sqrt{A-\boldsymbol{\sigma}:\boldsymbol{\varepsilon}_t a}$$
$$=\frac{\sqrt{2\beta}}{4}\sqrt{A_0(\theta-\theta_c)-\Delta G^{\theta}a}$$
$$=\frac{\sqrt{2\beta}}{4}\sqrt{(A_0-za)\theta+za\theta_e-A_0\theta_c}$$
$$=\frac{1}{4}\sqrt{\frac{a(6-a)\beta\varepsilon_t H}{3}};$$

$$E_6^{\mathrm{AM}}=3\sqrt{3\beta\tilde{G}_6(\eta_{63})}/4,\quad E_4^{\mathrm{AM}}=4\sqrt{\beta\tilde{G}_4(\eta_{43})}/3, \tag{69}$$

where $\tilde{G}_6(\eta_{63})=2s_1/27$ and $\tilde{G}_4(\eta_{43})=s_1/16$ are the energy barriers between A and M at thermodynamic equilibrium. Equation (69) expresses the A-M interface energy in terms of the material parameters and temperature (or stress, which is related to temperature via the equilibrium condition $s_2=0$), the stress hysteresis, or the energy barrier between A and M at thermodynamic equilibrium.

The interface thickness is defined by

$$\Delta^{\mathrm{AM}}:=\left(\frac{d\varphi[\eta(x)]}{dx}\right)^{-1}_{max}, \tag{70}$$

which results in

$$\Delta_4^{\mathrm{AM}}=\frac{(21-5a+K_4)^5}{32(a-6)^3[11a^3-81(9+K_4)-5a^2(24+K_4)+a(486+39K_4)]}\sqrt{\frac{\beta}{s_1}},$$
$$\Delta_6^{\mathrm{AM}}=\frac{(72-15a+K_6)^4}{128\sqrt{2}(a-6)^3[-27a^2-24(24+K_6)+5a(48+K_6)]}\sqrt{\frac{\beta}{s_1}}, \tag{71}$$
$$K_4:=\sqrt{81-30a+5a^2},\quad K_6:=\sqrt{576-240a+33a^2}.$$

Both Δ_4^{AM} and Δ_6^{AM} are complicated functions of a but they are accurately approximated by the polynomials

$$1.88\leqslant p_6=1.88+0.179a+0.00065a^2-0.0035a^3\leqslant 2.386,$$
$$2.411\leqslant p_4=-0.028(a-3)^2+2.667\leqslant 2.667. \tag{72}$$

The interface thicknesses are given by

$$\Delta_6^{\mathrm{AM}}=\frac{p_6}{p_4}\Delta_4^{\mathrm{AM}}=p_6\sqrt{\frac{\beta}{s_1}}=p_6\sqrt{\frac{\beta}{A_0(\theta-\theta_c)-\Delta G^{\theta}a}}$$
$$=p_6\sqrt{\frac{\beta}{(A_0-za)\theta+za\theta_e-A_0\theta_c}}$$
$$=\sqrt{6}p_6\sqrt{\frac{\beta}{a(6-a)\varepsilon H}};$$

$$\Delta_6^{\mathrm{AM}}=\frac{2}{3\sqrt{6}}p_6\sqrt{\frac{\beta}{\tilde{G}_6(\eta_{63})}},\quad \Delta_4^{\mathrm{AM}}=p_4\sqrt{\frac{\beta}{\tilde{G}_4(\eta_{43})}}. \tag{73}$$

If $A_0=za$, then the stress hysteresis, interface energy density, and interface thickness are temperature independent. It follows from Eqs. (69)–(73) that

$$\frac{E_6^{\mathrm{AM}}}{\Delta_6^{\mathrm{AM}}}=s_1\frac{\sqrt{2}}{4p_6},\quad E_6^{\mathrm{AM}}\Delta_6^{\mathrm{AM}}=\frac{\sqrt{2}}{4}p_6\beta;$$
$$\frac{E_4^{\mathrm{AM}}}{\Delta_4^{\mathrm{AM}}}=\frac{s_1}{3p_4},\quad E_4^{\mathrm{AM}}\Delta_4^{\mathrm{AM}}=\frac{p_4}{3}\beta. \tag{74}$$

The differences in the A-M interface profiles and energy densities between the 2-4-6 and 2-3-4 potentials are not significant.

D. Critical austenitic nuclei: A solitons on M

In this section we consider the case where only M exists as $x\to\pm\infty$. The integration constant g_0 must be a function of the parameters k_6 or k_4 in order to satisfy the boundary conditions $d\xi(\pm\infty)/dy=0$:

$$g_4-g_{40}=(k_4-\xi_4)(\xi_4-\xi_{A1})(\xi_4-\xi_{A2}),$$
$$\xi_{A1}=\frac{1}{2}(1-2k_4+\sqrt{1-2k_4})\geqslant 0,$$
$$\xi_{A2}=\frac{1}{2}(1-2k_4-\sqrt{1-2k_4})\leqslant 0, \tag{75}$$
$$g_6-g_{60}=(k_6^2-\xi_6^2)^2(\xi_6^2-\xi_A^2),\quad \xi_A=\sqrt{1-2k_6^2}.$$

The solutions of Eq. (52) are

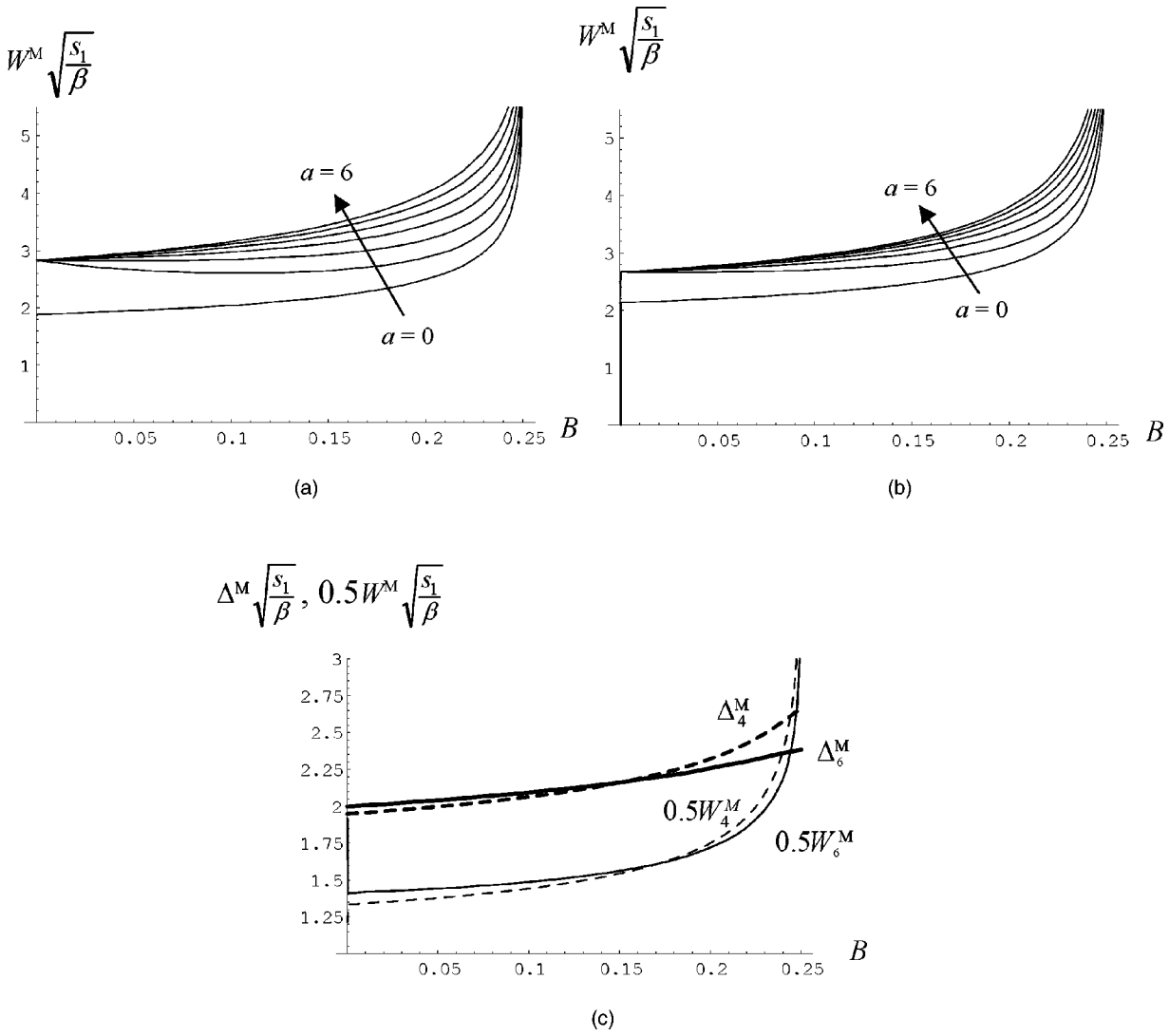

FIG. 12. The dimensionless effective widths $W^{M}\sqrt{s_1\beta}$ of the critical martensitic nuclei vs B for various values of a for (a) the 2-4-6 potential and (b) the 2-3-4 potential. (c) The dimensionless thickness $\Delta^{M}\sqrt{s_1/\beta}$ of the interface of a critical martensitic nucleus and half of the dimensionless effective width, $0.5W^{M}\sqrt{s_1/\beta}$, of a critical martensitic nucleus, both vs B for $a=3$. Solid (dashed) lines correspond to the 2-4-6 (2-3-4) polynomial.

$$\xi_6^{A}(y_6)=\frac{\xi_A}{\sqrt{1-\dfrac{3k_6^2-1}{k_6^2}\tanh^2(k_6\sqrt{3k_6^2-1}y)}},$$

$$\xi_4^{A}(y_4)=\frac{k_4(2-4k_4+H)}{-1+4k_4+H}, \tag{76}$$

$$H=\sqrt{1-2k_4}\times\cosh\left(\frac{1}{2}y_4\sqrt{1-\sqrt{1-2k_4}-4k_4}\sqrt{1+\sqrt{1-2k_4}-4k_4}\right).$$

The parameters k_6 and k_4 are restricted to the intervals $[1/\sqrt{3},1/\sqrt{2}]$ and $[3/8,1/2]$, respectively. It was proved numerically (as was done for the martensitic nucleus) that the solutions $\xi_6^{A}(y_6)$ and $\xi_4^{A}(y_4)$ describe critical austenitic nuclei (see Fig. 8). From Eq. (76) we obtain the physical order parameters as functions of P:

$$\eta_6^{A}(x)=\frac{\sqrt{P}}{\sqrt{2(3-P)-3(2-P)\tanh^2\left(\dfrac{1}{2}\sqrt{\dfrac{s_1}{\beta}}x\right)}}, \tag{77}$$

$$\eta_4^{A}(x)=1-\frac{6(2-P)}{4(3-P)+\sqrt{2P(6-P)}\cosh\left(\sqrt{\dfrac{s_1}{2\beta}(2-P)}x\right)},$$

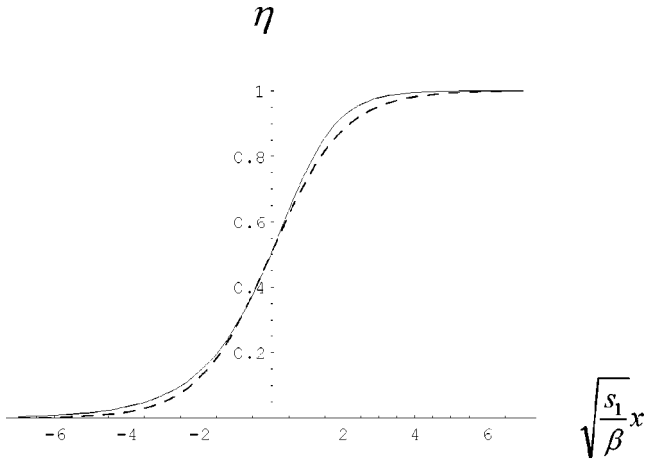

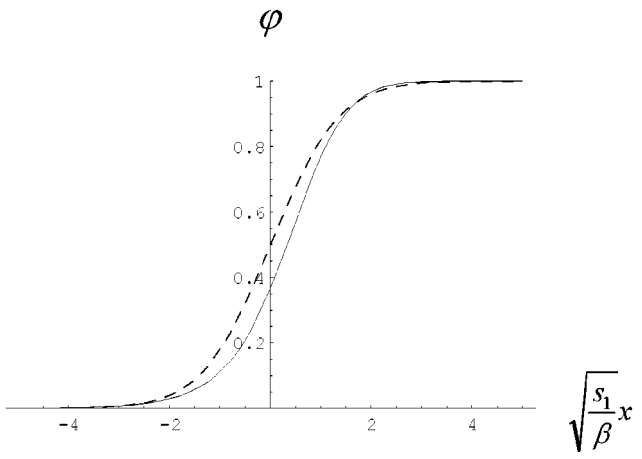

FIG. 13. Austenite-martensite diffuse interface profiles. Solid (dashed) lines correspond to the 2-4-6 (2-3-4) polynomial.

where $0 \leqslant P \leqslant 2$. The total energies per unit area of the critical nuclei are

$$E_4^{\mathsf{A}} = \frac{32}{27}\sqrt{\beta s_1}\frac{(6-P)^3}{(4-P)^{5/2}}e_4^{\mathsf{A}},$$

$$e_4^{\mathsf{A}} = 4\int_{\xi_{A1}}^{k_4}(\xi_4 - k_4)\sqrt{(\xi_4-\xi_{A1})(\xi_4-\xi_{A2})}\,d\xi_4$$

$$= \frac{1}{4(6-P)^3}\left[\frac{3}{2}(12-6P+P^2)\sqrt{2(4-P)(2-P)}\right.$$

$$\left. - P(3-P)(6-P)\ln\left(\frac{4(3-P)+3\sqrt{2(4-P)(2-P)}}{\sqrt{2P(6-P)}}\right)\right]$$

$$\simeq 0.083 - 0.086P + 0.024P^2 - 0.001P^3;$$

$$E_6^{\mathsf{A}} = \frac{3}{8}\sqrt{6\beta s_1}\frac{(4-P)^2}{(3-P)^{3/2}}e_6^{\mathsf{A}},$$

$$e_6^{\mathsf{A}} = 4\int_{\xi_A}^{k_6}(k_6^2-\xi_6^2)\sqrt{\xi_6^2-\xi_A^2}\,d\xi$$

$$= \frac{1}{2(4-P)}\left[\sqrt{\frac{2}{3}(3-P)(2-P)}\right.$$

$$\left. - \frac{P(8-3P)}{3(4-P)}\ln\left(\frac{\sqrt{2(3-P)}+\sqrt{3(2-P)}}{\sqrt{P}}\right)\right]$$

$$\simeq 0.248 - 0.227P + 0.046P^2 + 0.003P^3. \quad (78)$$

As was done for the martensitic nucleus, expressions for the width and interface thickness can be obtained for the austenitic nucleus.

Figure 10 shows the energies of the critical A nuclei for the 2-4-6 and 2-3-4 potentials versus α, and Fig. 14 shows profiles of the critical A nuclei for these two potentials. The results for the two potentials are very similar except for the widths in the neighborhood of $P=0$ where the 2-3-4 nucleus is significanlty narrower than the 2-4-6 nucleus.

E. Kink solutions: M-M interfaces and barrierless nucleation of austenite

In this section we present two M-M kink solutions of the static Ginzburg-Landau equations. The first is a solution for the potentials in hyperspherical coordinates, and the second is a M_+-M_- solution of the extended ($\eta \in [-1,1]$) 2-4-6 Landau potential that exhibits barrierless nucleation of austenite.

The minimum-energy paths between stable martensitic variants for the potentials in hyperspherical coordinates are great circles on the unit hypersphere, $r=1$. Kink solutions between martensitic variants exist when both variants have the same energy, which implies zero stress or zero transformation work. The potential along the great circle from M_i to any other variant is $G = \bar{A}\psi^2(1-\psi)^2 + \Delta G^{\theta}$ for both potentials. Both variants are twin-related IPS variants, $\boldsymbol{\varepsilon}_t(\psi) = \frac{1}{2}\gamma_t[-1+2\psi^2(3-2\psi)](\boldsymbol{mn}+\boldsymbol{nm}) + \varepsilon \boldsymbol{nn}$ [see Eqs. (20) and (27)]; that is, the normal strain is constant, the shear strain varies from $-\gamma_t$ to γ_t, and the PT does not proceed through A. The solution of the static Ginzburg-Landau equation $\partial G/\partial\psi = 2\beta\partial^2\psi/\partial x^2$ is

$$\psi = (1+\exp[-\sqrt{\bar{A}/\beta}(x-x_0)])^{-1}, \quad (79)$$

which interpolates between M_i at $-\infty$ and $\mathsf{M}_{j\neq i}$ at $+\infty$. The solution (79) coincides with Eq. (68) for $\eta_4^{\mathsf{AM}}(x)$ when s_1 is substituted for $\bar{A}$. For $a=3$, $P(\psi)=\varphi_4(\psi)$; thus the thickness of the interface is given by Eqs. (72) and (73) for Δ_4^{AM} with $s_1 \to \bar{A}$: $\Delta_{\psi}^{\mathsf{MM}} = 2.667\sqrt{\beta/\bar{A}}$. The total kink energy per unit area is $E_{\psi}^{\mathsf{MM}} = \sqrt{\beta\bar{A}}/3$.

The static Ginzburg-Landau equation for the 2-4-6 potential admits a kink solution such that $\eta(+\infty)=+1$, $\eta(-\infty)=-1$; i.e., the structure goes to M_+ as $x \to +\infty$ and to M_- as $x \to -\infty$. There is no corresponding solution for the 2-3-4 potential, so we can drop the subscript "6." Equation (75)

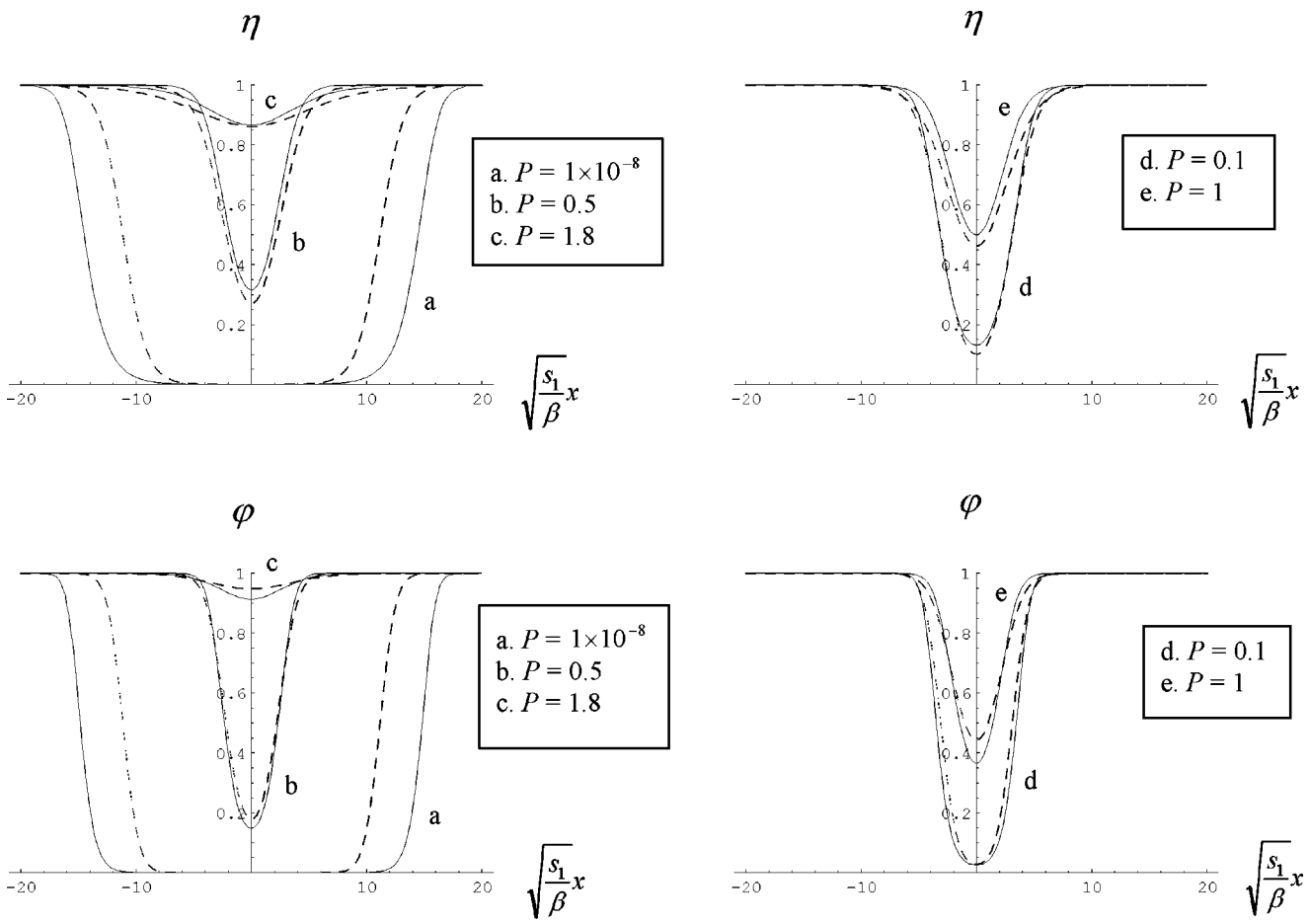

FIG. 14. Profiles of critical austenitic nuclei for various P and $a=2.98$. Solid (dashed) lines correspond to the 2-4-6 (2-3-4) polynomial.

remains valid but with imaginary ξ_A. It is convenient to designate an imaginary root of the equation $g=g_0$ as $\xi_A i$; then,

$$g-g_0=(k^2-\xi^2)^2(\xi^2+\xi_A^2),\quad \xi_A=\sqrt{2k^2-1}. \tag{80}$$

The solution of Eq. (52) is

$$\xi(y)=\frac{k\sinh(k\sqrt{3k^2-1}y)}{\sqrt{\dfrac{3k^2-1}{2k^2-1}+\sinh^2(k\sqrt{3k^2-1}y)}},$$
$$\eta(x)=\frac{\sinh\left(\sqrt{\dfrac{s_1(2-P)}{\beta}}\dfrac{x}{2}\right)}{\sqrt{3\left(1-\dfrac{2}{P}\right)+\sinh^2\left(\sqrt{\dfrac{s_1(2-P)}{\beta}}\dfrac{x}{2}\right)}}. \tag{81}$$

This solution is valid for $P\leqslant 0$, $0\leqslant B\leqslant 1/4$. Since $\boldsymbol{\sigma}:\boldsymbol{\varepsilon}_t=0$, it follows that $P=12\Delta G^\theta/A$; hence $\Delta G^\theta\leqslant 0$ since $P\leqslant 0$, which implies stability of M and metastability of A, or equilibrium. The profiles $\eta(x)$ and $\varphi[\eta(x)]$ for various P are shown in Fig. 15. The total energy per unit area of the M_+-M_- interface is

$$E^{MM}=\frac{1}{k^2}\sqrt{\frac{\beta s_1}{2B}}e^{MM},$$
$$e^{MM}=4\int_0^k(k^2-\xi^2)\sqrt{\xi^2+\xi_A^2}\,d\xi \tag{82}$$
$$=\frac{1}{2}\left[k\sqrt{3k^2-1}+(1-8k^2+12k^4)\ln\left(\frac{k+\sqrt{3k^2-1}}{\sqrt{2k^2-1}}\right)\right].$$

Figure 10 shows $E^{MM}/\sqrt{\beta s_1}$ versus α. Note that $E^{MM}/\sqrt{\beta s_1}\to\infty$ when $B\to 0$ $(\alpha\to -1)$; however, $s_1/B\to -3s_2/4$ and $E^{MM}/\sqrt{\beta}\to 0.901\sqrt{-s_2}=3.12\sqrt{-\Delta G^\theta}$ in the same limit. When $P\to 0$, $E^{MM}/\sqrt{\beta}\to\sqrt{s_1/2}=\sqrt{A/2}$. The energy of the M_+-M_- interface and the energies of the critical A and M nuclei all coincide when A and M are in thermodynamic equilibrium.

It is convenient to introduce the dimensionless temperature $T:=(\theta_e-\theta)/(\theta_e-\theta_c)$, $0\leqslant T\leqslant 1$. Then $s_1=A=A_0(\theta_e-\theta_c)(1-T)$ and $P=12zT/[A_0(T-1)]$. Plots of $E^{MM}/\sqrt{\beta A_0(\theta_e-\theta_c)}$ vs T for various values of $0\leqslant A_0/12z\leqslant 1/2$ are shown in Fig. 16.

As was mentioned in Ref. 11 and 12, soliton splitting occurs (Fig. 15) as the A-M equilibrium line is approached $(B\to 1/4, P\to 0)$; that is, the M_+-M_- diffuse interface splits into M_+-A and A-M_- diffuse interfaces separated by an A

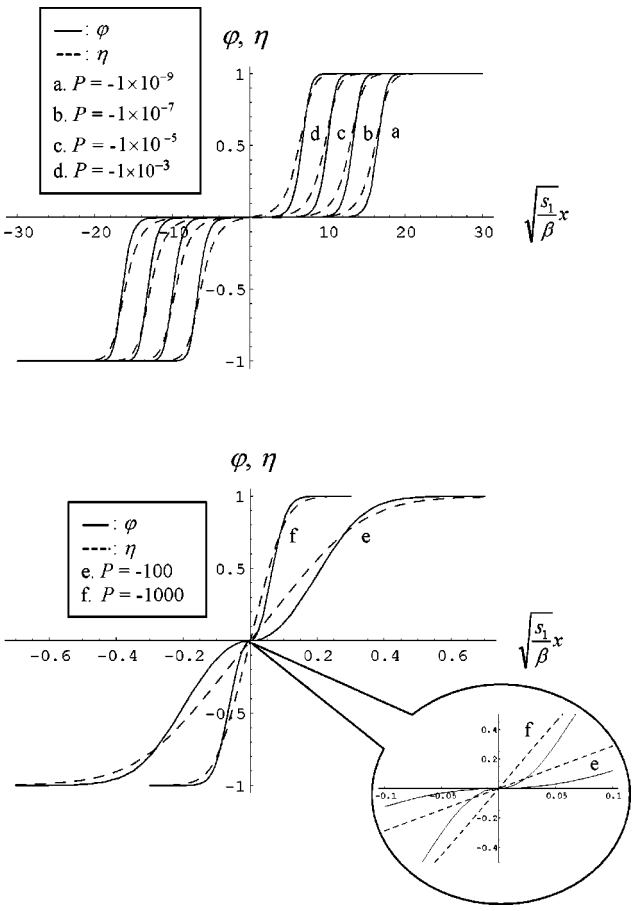

FIG. 15. M_--M_+ interface profiles for various P.

region. As $P\to 0^-$ the solution (81) for $\eta(x)$ assumes the form $\mathrm{sgn}(x)/\{1+6/[|P|\sinh^2(\sqrt{s_1/2\beta}x)]\}^{1/2}$, whose magnitude is less than or equal to δ for $|x|\leqslant x_\delta$, where $x_\delta = \sqrt{\beta/2s_1}\ln(24\delta^2/|P|)$ for $\sqrt{|P|}\ll\delta\ll 1$; the width of the austenitic region grows logarithmically as the equilibrium line is neared.

The thickness of the M_+-M_- interface can be estimated for $P\leqslant -1$ by the expression

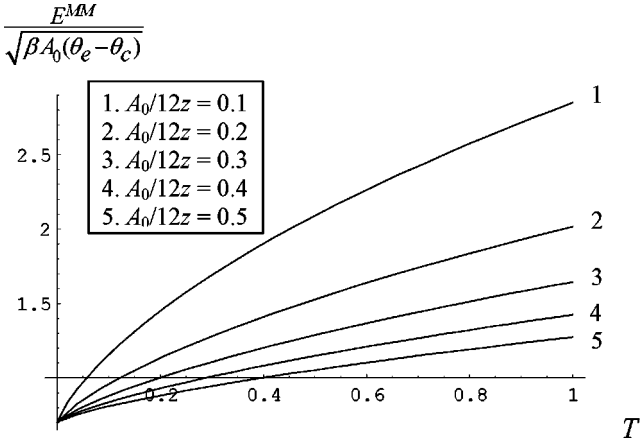

FIG. 16. M_--M_+ dimensionless interface energy $E^{\mathsf{MM}}/\sqrt{\beta A_0(\theta_e-\theta_c)}$ vs dimensionless temperature T for various values of $A_0/12z$.

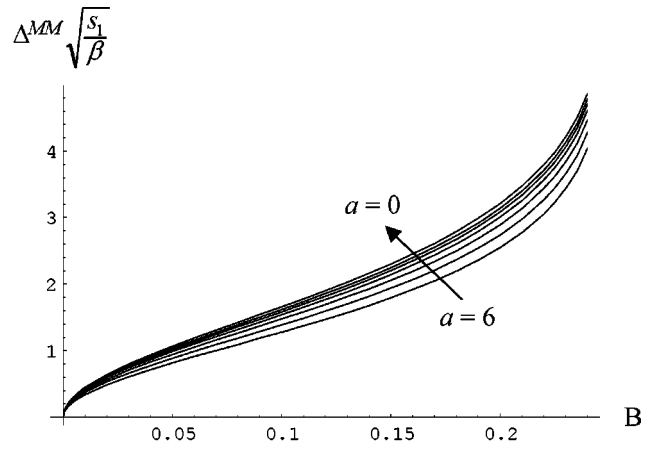

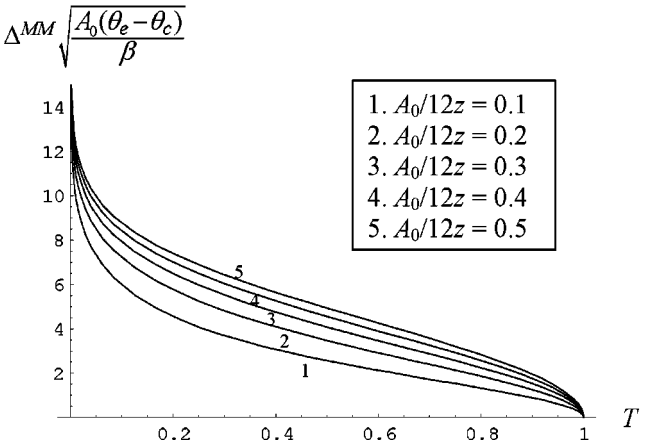

FIG. 17. (a) The M_--M_+ dimensionless interface width $\Delta^{\mathsf{MM}}\sqrt{s_1/\beta}$ vs B for various a. (b) the M_--M_+ dimensionless interface width $\Delta^{\mathsf{MM}}\sqrt{A_0(\theta_e-\theta_c)/\beta}$ vs dimensionless temperature T for $a=2.98$ and various values of $A_0/12z$.

$$\Delta^{\mathsf{MM}} := 2x_{0.95} = \sqrt{\beta/s_1}\,\frac{4}{\sqrt{2-P}}\sinh^{-1}\left(\eta_{0.95}\sqrt{-\frac{3(2-P)}{(1-\eta_{0.95}^2)P}}\right),$$

$$\eta_{0.95} = 0.931 - 0.011a + 0.003a^2 - 0.000\,08a^3. \qquad (83)$$

Here $x_{0.95}$ is defined by the condition $\varphi[\eta(x_{0.95})]=0.95$. Equation $(83)_1$ was obtained from the condition $\eta(x_{0.95}) = \eta_{0.95}$ using Eq. $(81)_2$. The function $\eta_{0.95}(a)$ was determined by numerical solution of the equation $\varphi(\eta_{0.95}) = 0.95$ and then approximated by the cubic polynomial, Eq. $(83)_2$. Plots of $\Delta^{\mathsf{MM}}\sqrt{s_1/\beta}$ vs B for various a and $\Delta^{\mathsf{MM}}\sqrt{A_0(\theta_e-\theta_c)/\beta}$ vs T for $a=2.98$ (NiAl value) and various values of $0\leqslant A_0/12z\leqslant 1/2$ are shown in Fig. 17. For $P\geqslant -1$ the splitting is so pronounced that we no longer have an interface in the usual sense of the word. Equation (83) then gives the width of the austenitic nucleus.

Near the A-M equilibrium line, $0<k^2-1/2\ll 1$, and Eq. (81) for the order parameter becomes

$$\xi(y)=\sqrt{2}\sinh(y/2)[\exp(y_0)+4\sinh^2(y/2)]^{-1/2},$$

$$y_0=-\ln(k^2-1/2). \tag{84}$$

Now expand the hyperbolic sine around $y_0 \gg 1$, $\sinh(y/2) \approx \exp(y_0/2)\exp[(y-y_0)/2]/2$, and substitute into Eq. (84):

$$\xi(y)=[2(1+e^{-(y-y_0)})]^{-1/2}. \tag{85}$$

This is identical to ξ_6^{AM} [see Eq. (68)], the A-M diffuse interface, as expected.

Austenite nucleation inside a homogeneous, thermodynamically stable martensitic phase is suppressed by the large activation energy [see Eq. (78)] required to form an unstable critical nucleus. In contrast, the formation of an A region between the M_+ and M_- occurs with no cost in energy. Soliton splitting is a barrierless mechanism for A nucleation in the region of M stability. A stable austenitic nucleus is formed and grows as the temperature approaches the equilibrium temperature, and expands to infinity at the equilibrium temperature. Note that for $P \ll 0$, when the A embryo is not visible in the $\eta(x)$ profile in Fig. 15, it can be seen in the $\varphi(x)$ profile; this is because $d\eta(0)/dx \neq 0$ but $d\varphi[\eta(0)]/dx=[d\varphi(0)/d\eta][d\eta(0)/dx]=0$. We believe that such a mechanism may be observable in experiments on three-dimensional systems when the transformation strain is an IPS (to avoid distortion along the interface). This may be the case for the interface between two IPS variants for any PT.

VI. NIAL CUBIC-TETRAGONAL PT: M-M AND M-A INTERFACES

Let us estimate the parameter β for NiAl alloys. The transformation strain for a variant-variant transformation in NiAl is an IPS and the transformation does not pass through A, so our results for M-M interfaces in polar coordinates are applicable to NiAl. Taking $\overline{A}=5320$ MPa [Eq. (39)] one obtains

$$E_\psi^{\mathsf{MM}}=2.43\times 10^4\sqrt{\beta}\ N^{1/2}\mathrm{m}^{-1},$$
$$\Delta_\psi^{\mathsf{MM}}=6.22\times 10^{-5}\sqrt{\beta}\ N^{-1/2}\mathrm{m}. \tag{86}$$

High-resolution electron microscopy[13] of $Ni_{65}Al_{35}$ (the data that we used in Ref. 2 and in Sec. IV are for $Ni_{61}Al_{39}$) brackets the width of the martensite-martensite interface between one and several interatomic distances (see Figs. 5 and 6 in Ref. 13). If we assume $\Delta_\psi^{\mathsf{MM}}=0.3\times 10^{-9}$ m, which corresponds to an interatomic distance, then we obtain $\beta=2.33\times 10^{-11}$ N and $E_\psi^{\mathsf{MM}}=0.117\ \mathrm{J\,m^{-2}}$ from Eq. (86). This value for β gives $\Delta_6^{\mathsf{AM}}=0.243\times 10^{-9}$ m from Eq. (73) and $E_6^{\mathsf{AM}}=0.079\ \mathrm{J/m^2}$ from Eq. (74) for the stress-free case at $\theta=300$ K. If we take $\Delta_\psi^{\mathsf{MM}}=10^{-9}$ m, then $\beta=2.588\times 10^{-10}$ N, $E_\psi^{\mathsf{MM}}=0.391\ \mathrm{J\,m^{-2}}$, $\Delta_6^{\mathsf{AM}}=0.809\times 10^{-9}$ m, and $E_6^{\mathsf{AM}}=0.263\ \mathrm{J/m^2}$ from Eq. (74). If the surface energy is known, then a more precise estimate of β can be made using Eq. (86) or Eqs. (73) and (74).

Note that the relatively high value of E_6^{AM} in comparison to $0.01-0.02\ \mathrm{Jm^{-2}}$ for steels is related to the very high barriers for stress-induced PT, i.e., $\overline{A}$ and $A_0(\theta_e-\theta_c)$. Our Eq. (69) for E_4^{AM} in terms of $\tilde{G}_4(\eta_{43})$, the energy barrier between A and M at thermodynamic equilibrium, exactly coincides with the corresponding equation in Ref. 7 because Eq. (69) is independent of stress, and at zero stress and for one M variant both Gibbs potentials coincide. Our value for Δ_4^{AM} at $a=2.98$ is 0.667 of the corresponding value in Ref. 7.

VII. PHASE FIELD THEORY OF DISLOCATIONS

In this section we discuss a serious shortcoming of the present-day phase field theory of dislocations and then demonstrate that this drawback can be eliminated by following an approach similar to the one we used to construct our Landau potentials.

In the phase field theory of dislocations (see, e.g., Ref. 3) the Burgers vector and consequently the plastic strain depend on the applied stress even in the elastic regime—that is, when dislocations are in stable equilibrium and no plastic flow occurs. Such a dependence is in conflict with the definition of plastic strain in macroscopic plasticity theory. A $\boldsymbol{\sigma}$-dependent Burgers vector is inconsistent with the well-established theory of dislocations.[14] It also implies dissipation during elastic deformation of plastically deformed material.[10] The $\boldsymbol{\sigma}$ dependence of the plastic strain in the phase field theory is analogous to the $\boldsymbol{\sigma}$ dependence of the transformation strain in Landau theories of PT's; see analysis in Ref. 1.

Consider one slip plane and one slip direction—i.e., one Burgers vector $\boldsymbol{b}$. Then Eqs. (3) and (4) in Ref. 3 for the Burgers vector and plastic strain reduce to $\boldsymbol{b}(\eta)=\boldsymbol{b}\eta$ and $\boldsymbol{\varepsilon}_p(\eta)=\boldsymbol{bn}\eta/d=\boldsymbol{\varepsilon}_p\eta$, where η is the density function (phase field) for dislocations, $\boldsymbol{n}$ is the normal to the slip plane, and d is the distance between the slip planes. The local potential of the crystal lattice [Eq. (8) in Ref. 3] is $f=A\sin^2(\pi\eta)$, which leads to the Gibbs potential $G=-\boldsymbol{\sigma}:\boldsymbol{\lambda}:\boldsymbol{\sigma}/2-\boldsymbol{\sigma}:\boldsymbol{\varepsilon}_p(\eta)+A\sin^2(\pi\eta)$. The corresponding equation of thermodynamic equilibrium is $\partial G/\partial\eta=0=-\boldsymbol{\sigma}:\boldsymbol{\varepsilon}_p+\pi A\sin(2\pi\eta)$; hence $2\pi\eta=\arcsin[\boldsymbol{\sigma}:\boldsymbol{\varepsilon}_p/(\pi A)]+n$, where $n=0,1,2,\ldots$ is the number of dislocations. Therefore, in thermodynamic equilibrium, the order parameter η, the Burgers vector $\boldsymbol{b}(\eta)$, and plastic strain $\boldsymbol{\varepsilon}_p(\eta)$ depend on the stress $\boldsymbol{\sigma}$. We can avoid this unphysical dependence on $\boldsymbol{\sigma}$ by first breaking the order parameter into an integer part $\mathrm{Int}(\eta)$ and a fractional part $\overline{\eta}:=\eta-\mathrm{Int}(\eta)\in[0,1]$, and then incorporating the dependence on $\overline{\eta}$ through the 2-3-4 or 2-4-6 polynomials $\varphi(\eta)$, as was done for the transformation strain in our Landau potentials:

$$\boldsymbol{b}(\eta)=\boldsymbol{b}[\varphi(\overline{\eta})+\mathrm{Int}(\eta)],\quad \boldsymbol{\varepsilon}_p(\eta)=\boldsymbol{bn}[\varphi(\overline{\eta})+\mathrm{Int}(\eta)]/d. \tag{87}$$

The term $\mathrm{Int}(\eta)=n$ accounts for the presence of n dislocations in the slip plane, each with Burgers vector $\boldsymbol{b}$. The Gibbs potential for three shear stresses is shown in Fig. 18. The thermodynamic equilibrium condition $\partial G/\partial\eta=0$ has the

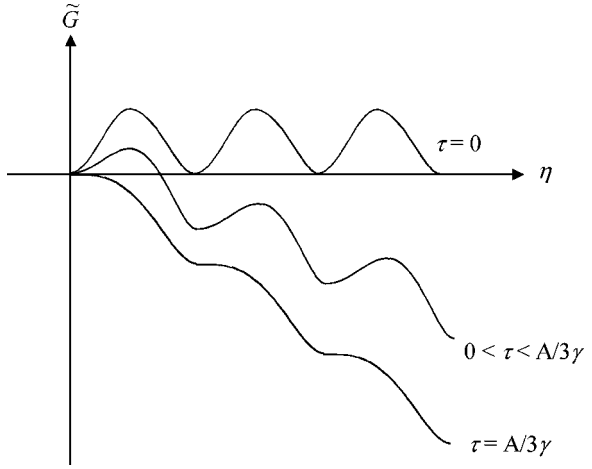

FIG. 18. Gibbs potential $\tilde{G}$ for dislocations for three shear stresses.

roots $\eta = n (n = 1,2,3, \ldots)$ corresponding to thermodynamic equilibrium of n dislocations. It also has the roots $\bar{\eta}_3$ of the equation

$$\boldsymbol{\sigma}:\boldsymbol{\varepsilon}_p \frac{d\varphi(\bar{\eta}_3)}{d\eta} = \pi A \sin(2\pi\bar{\eta}_3) \tag{88}$$

corresponding to the maxima of $G(\boldsymbol{\sigma}, \theta, \eta)$, which represent the activation barriers to the dislocation motion. An analytical solution for $\bar{\eta}_3$ cannot be found, but if $f = A\sin^2(\pi\eta)$ is replaced by periodic 2-3-4 or 2-4-6 crystal potentials in η, for example,

$$f_4(\bar{\eta}) = A\bar{\eta}^2(1-\bar{\eta})^2, \quad f_6(\bar{\eta}) = A\bar{\eta}^2(1-\bar{\eta}^2)^2/2, \tag{89}$$

then analytic solutions can be obtained. For the crystal potentials (89) our Gibbs potential in $\bar{\eta}$ is identical in form to the $G(\eta)$ for twinning, so we can use all of the results previously obtained for twinning. In particular, for $a = 3$,

$$\bar{\eta}_{43} = (A - 3\boldsymbol{\sigma}:\boldsymbol{\varepsilon}_p)/2A, \quad \bar{\eta}_{63} = \sqrt{A - 3\boldsymbol{\sigma}:\boldsymbol{\varepsilon}_p}/\sqrt{3(A + \boldsymbol{\sigma}:\boldsymbol{\varepsilon}_p)}. \tag{90}$$

We write $\boldsymbol{\sigma}:\boldsymbol{\varepsilon}_p = \tau\gamma_p$ with $\tau = \mathbf{b}\cdot\boldsymbol{\sigma}\cdot\mathbf{n}/|\mathbf{b}|$ the resolved shear stress and $\gamma_p = |\mathbf{b}|/d$ the plastic shear strain. The equilibrium $\tau - \bar{\eta}$ curve can be obtained from Eq. (90):

$$\tau_4 = \frac{A}{3\gamma}(1 - 2\bar{\eta}), \quad \tau_6 = \frac{A}{3\gamma}\frac{1 - 3\bar{\eta}^2}{1 + \bar{\eta}^2}. \tag{91}$$

The condition for loss of stability of a dislocation and its barrierless motion—namely, $\tau \geqslant A/3\gamma$ (see Fig. 18)—is the same for both polynomials. Reverse motion occurs for $\tau \leqslant -A/3\gamma$. The generalization to multiple slip systems can be effected by means of the approach followed in Ref. 3.

VIII. CONCLUDING REMARKS

The most significant difference between the 2-3-4-5 and 2-4-6 potentials is that the ratio of the curvature of the M minimum to the curvature of the A minimum is 4 times greater for the 2-4-6 potential: $[\partial^2 G_4(1)/\partial\eta^2]/[\partial^2 G_4(0)/\partial\eta^2] = 1 - P/2$ and $[\partial^2 G_6(1)/\partial\eta^2]/[\partial^2 G_6(0)/\partial\eta^2] = 4(1 - P/2)$. The critical M nucleus is particularly sensitive to the larger curvature at the M minimum of the 2-4-6 potential. For example, its amplitude is larger for the 2-4-6 potential; especially near the M instability line, its width is larger for the 2-3-4 potential when $B > 0.17$, and its energy is greater for the 2-4-6 potential. On the other hand, the energy and amplitude of the critical A nucleus are nearly the same for both potentials, and the profiles, widths, and energies of the A-M interfaces are very similar. Despite the fact that all phase equilibrium and transformation conditions are the same for both potentials for a homogeneous distribution of order parameter, the difference in curvature does affect the energetics and relative stability of phases for a nonuniform distribution.

Note that our potentials do not have parameters that control the relative curvatures of $G(\eta)$ at the A and M minima. We remind the reader that these curvatures are not related to elastic moduli, as is the case for Landau potentials with strain-based order parameters. We plan to generalize our potentials by introducing additional parameters that control the curvatures at the A and M minima and study the effect of variations in these parameters on critical nuclei and interfaces. The actual values of these parameters can be determined from the results of atomistic calculations.

In this paper we considered only homogeneous nucleation—that is, nucleation in defect-free crystals or parts of crystals: nanocrystals, thin films, or nanoprecipitates. Our results can be used to approximately model the nonclassical nucleation of an ellipsoidal region, which was carried out in Ref. 7, but more precisely and with allowance for applied stresses. Heterogeneous nucleation at various dislocation configurations (pileups, low- and high-angle boundaries), as well as generation of dislocations during PT's can be studied using a combination of the phase field theories of PT's and dislocations developed in this paper.

The free surface boundary condition $d\eta/dx = 0$ is satisfied at the maxima of the A and M critical nuclei. Consequently, a critical nucleus at a free surface is simply half of a critical nucleus in the bulk. Since the energy of a surface nucleus is half of the energy of the corresponding nucleus in bulk, the probability of its appearance is significantly higher.

We plan to obtain and compare analytical and numerical solutions of the time-dependent Ginzburg-Landau equations for the 2-3-4-5 and 2-4-6 potentials. We also plan to develop a generalization of our Landau theory for large strains and large material rotation, a very challenging problem. Such a generalization is essential for PT's with components of transformation strain exceeding 0.1 and for loadings that are accompanied by finite rotations of the crystal lattice.

ACKNOWLEDGMENTS

Support of Los Alamos National Laboratory for V.I.L. under consulting agreement No. C-8060 and for V.I.L. and D.W.L. under Contract No. 52844 is gratefully acknowledged. V.I.L. also acknowledges NSF support (Grant No. CMS-02011108) and D.W.L. also acknowledges support of the ME Department of Texas Tech University. We would like to thank Dr. D. Schryvers for providing and discussing his data on the thickness of the variant-variant interface in NiAl.

*FAX: (253) 679 8926. Electronic address: valery.levitas @coe.ttu.edu

[1] V.I. Levitas and D.L. Preston, Phys. Rev. B **66**, 134206 (2002).
[2] V.I. Levitas and D.L. Preston, Phys. Rev. B **66**, 134207 (2002).
[3] Y.U. Wang, Y.M. Jin, A.M. Cuitiño, and A.G. Khachaturyan, Acta Mater. **49**, 1847 (2001).
[4] A. Artemev, Y. Jin, and A.G. Khachaturyan, Acta Mater. **49**, 1165 (2001).
[5] F. Falk, Z. Phys. B: Condens. Matter **51**, 177 (1983).
[6] A.E. Jacobs, Phys. Rev. B **46**, 8080 (1992).
[7] D.M. Haezebrouck, Ph.D. thesis, Northwestern University, 1987.
[8] F. Falk and P. Konopka, J. Phys.: Condens. Matter **2**, 61 (1990).
[9] K. Bhattacharyya and R.V. Kohn, Acta Mater. **4**, 529 (1996).
[10] V.I. Levitas, *Large Deformation of Materials with Complex Rheological Properties at Normal and High Pressure* (Nova Science, New York, 1996).
[11] A.E. Jacobs, Phys. Rev. B **31**, 5984 (1985).
[12] J. Lajzerkowicz, Ferroelectrics **35**, 219 (1981).
[13] Ph. Boullay, D. Schryvers, and J.M. Ball, Acta Mater. **51**, 1421 (2003).
[14] J. P. Hirth and J. Lothe, *Theory of Dislocations* (Krieger, Malabar, FL, 1992).